JACS
JOURNAL OF THE AMERICAN CHEMICAL SOCIETY

ARTICLE

pubs.acs.org/JACS

Synthesis and Electronic Structure Determination of *N*-Alkyl-Substituted Bis(imino)pyridine Iron Imides Exhibiting Spin Crossover Behavior

Amanda C. Bowman,[†,‡] Carsten Milsmann,[†,‡,§] Eckhard Bill,[‡] Zoë R. Turner,[§] Emil Lobkovsky,[†] Serena DeBeer,[†,‡] Karl Wieghardt,[‡] and Paul J. Chirik*[,†,§]

[†]Department of Chemistry and Chemical Biology, Baker Laboratory, Cornell University, Ithaca, New York 14853, United States

[‡]Max-Planck Institute for Bioinorganic Chemistry, Stiftstrasse 34-36, D-45470 Mülheim an der Ruhr, Germany

[§]Department of Chemistry, Princeton University, Princeton, New Jersey, 08544, United States

Supporting Information

ABSTRACT: Three new *N*-alkyl substituted bis(imino)-pyridine iron imide complexes, (^{iPr}PDI)FeNR (^{iPr}PDI = 2,6-(2,6-^{i}Pr$_2$–C$_6$H$_3$–*N*=CMe)$_2$C$_5$H$_3$N; R = 1-adamantyl (^{1}Ad), cyclooctyl (^{Cy}Oct), and 2-adamantyl (^{2}Ad)) were synthesized by addition of the appropriate alkyl azide to the iron bis(dinitrogen) complex, (^{iPr}PDI)Fe(N$_2$)$_2$. SQUID magnetic measurements on the isomeric iron imides, (^{iPr}PDI)FeN^{1}Ad and (^{iPr}PDI)FeN^{2}Ad, established spin crossover behavior with the latter example having a more complete spin transition in the experimentally accessible temperature range. X-ray diffraction on all three alkyl-substituted bis(imino)pyridine iron imides established essentially planar compounds with relatively short Fe–N$_{imide}$ bond lengths and two-electron reduction of the redox-active bis(imino)pyridine chelate. Zero- and applied-field Mössbauer spectroscopic measurements indicate diamagnetic ground states at cryogenic temperatures and established low isomer shifts consistent with highly covalent molecules. For (^{iPr}PDI)FeN^{2}Ad, Mössbauer spectroscopy also supports spin crossover behavior and allowed extraction of thermodynamic parameters for the $S = 0$ to $S = 1$ transition. X-ray absorption spectroscopy and computational studies were also performed to explore the electronic structure of the bis(imino)pyridine alkyl-substituted imides. An electronic structure description with a low spin ferric center ($S = 1/2$) antiferromagnetically coupled to an imidyl radical ($S_{imide} = 1/2$) and a closed-shell, dianionic bis(imino)pyridine chelate ($S_{PDI} = 0$) is favored for the $S = 0$ state. An iron-centered spin transition to an intermediate spin ferric ion ($S_{Fe} = 3/2$) accounts for the $S = 1$ state observed at higher temperatures. Other possibilities based on the computational and experimental data are also evaluated and compared to the electronic structure of the bis(imino)pyridine iron *N*-aryl imide counterparts.

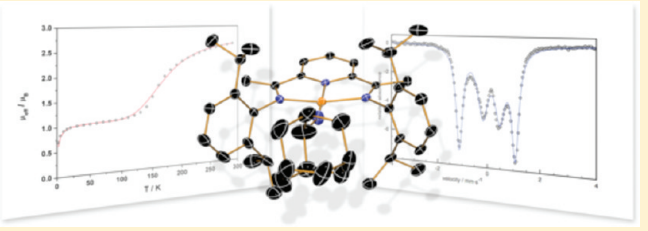

INTRODUCTION

Terminal iron imido compounds, L$_n$FeNR, once rare, have attracted renewed attention due to their interesting electronic structures, unique reactivity, and importance as model compounds for metalloenzymes and nitrogen fixation.[1] These compounds, owing to their higher d-electron counts, offer opportunities for catalytic chemistry resulting from the relative destabilization (viz. reduction in bond order) of the iron–nitrogen bond.[1,2] Following Lee's preparation and characterization of a tetranuclear iron cubane structure with an Fe=N^{t}Bu linkage,[3] a host of iron imido complexes has since been prepared and fully characterized. Examples are now known with oxidation states ranging from Fe(II) to Fe(V)[4] with a variety of spin states.

Four-coordinate, pseudotetrahedral iron imides are by far the most prominent coordination geometry because the π-antibonding orbitals with respect to the Fe–N bonds are empty. Low-spin Fe(II)[5] and Fe(III)[6] examples with tridentate tris(phosphino)-borate ligands have been thoroughly studied by Peters and co-workers. A cationic iron(IV) example has also been isolated by replacing one of the phosphine arms with a pyrazolyl donor.[7] Modification of the tris-phosphine ligand architecture has since continued, and five-coordinate iron compounds with axial silyl[8]- and borane[9]-tethers have been synthesized to enforce trigonal bipyramidal coordination.

The pseudotetrahedral examples exhibit rich reaction chemistry including N–H bond formation and ultimately aniline dissociation following addition of H$_2$.[10] Smith and co-workers have also explored pseudotetrahedral, neutral iron(III) and cationic iron(IV) imides with a tripodal tris(*N*-heterocyclic carbene)borato ligand. The iron(IV) example promotes hydrogen atom transfer of weak C–H bonds such as those in 9,10-dihydroanthracene allowing construction of a thermodynamic cycle and determination of the N–H bond dissociation energy as 88(5) kcal/mol.[11]

Three-coordinate, metastable, yet isolable, iron(III) imides bearing β-diketiminate ligands have been reported by Holland

Received: June 20, 2011
Published: October 10, 2011

Scheme 1. Preparation and Hydrogenation Chemistry of (^{iPr}PDI)Fe=NAr Compounds

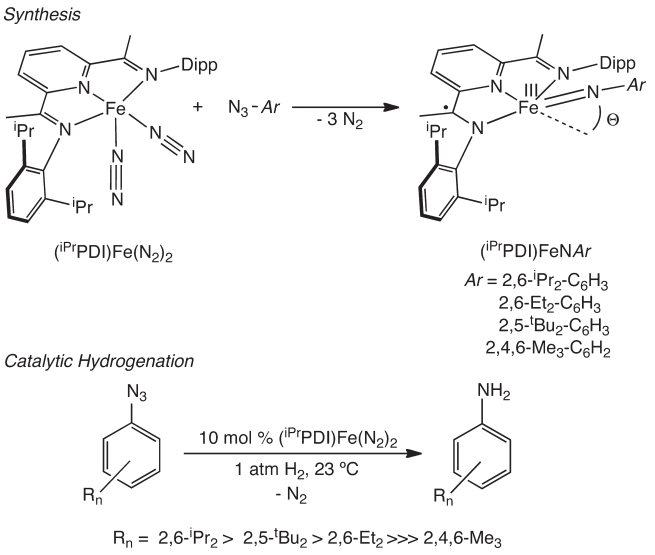

and co-workers.[12,13] Spectroscopic, structural, and computational characterization have established $S = 3/2$ ground states with short Fe=NR bonds of 1.68 Å and a formal Fe−N bond order of 2.5.[12] Addition of a fourth ligand such as *tert*-butyl pyridine resulted in C−H bond activation chemistry by hydrogen atom transfer.[12,14,15] Other notable reactivity includes reductive coupling to form an unusual diiron(II) hexazene compound[16] and catalytic group transfer reactions with isocyanides and carbon monoxide.[17] Using a related but weaker field monoanionic, bidentate dipyrromethane ligand scaffold, Betley and co-workers have also explored the synthesis and reactivity of the corresponding iron imide compounds.[18,19] Inclusion of a chloride ligand renders the *formal* oxidation state one unit higher than the analogous four-coordinate β-diketiminate examples. The original examples promote intramolecular C−H activation of a ligand substituent,[18] and modification of the dipyrromethane and imide architectures has resulted in iron compounds that are active for the catalytic, intermolecular amination of a benzylic C−H bond of toluene and the aziridination of styrene.[19] Spectroscopic, structural, and computational studies support ferric compounds with an imido-based radical, a bonding motif first positively identified in chromium chemistry.[20] Hydrogen atom abstraction by a putative Fe(IV) imide has also been postulated by Borovik and co-workers following treatment of a four-coordinate ureate/amidate complex with aryl azides.[21]

Our laboratory has been investigating the chemistry of reduced iron and cobalt compounds in the context of base-metal catalysis[22,23] and studying fundamental transformations relevant to small-molecule activation with redox-active bis(imino)pyridine ligands.[24,25] Because this class of chelate is tridentate and prefers meridional ligation, we sought to explore the synthesis and electronic structure of square-planar iron imido complexes, a geometry and ligand field distinct from the other classes of known L_nFeNR compounds. These complexes may ultimately prove more reactive, as $d\pi^*$ orbitals with respect to the Fe−N bond will likely be populated. Treatment of the bis(imino)pyridine iron bis(dinitrogen) complex, (^{iPr}PDI)Fe(N_2)$_2$ (^{iPr}PDI = 2,6-(2,6-^{i}Pr$_2$−C_6H_3−N=CMe)$_2C_5H_3N$),[22] with sterically hindered aryl azides, ArN_3 (Ar = 2,6-^{i}Pr$_2$-C_6H_3, 2,6-Et$_2$-C_6H_3, 2,4,6-Me$_3$-C_6H_2, or 2,5-^{t}Bu-C_6H_3), furnished the *N*-aryl substituted imido complexes, (^{iPr}PDI)FeNAr.[26] A combination of solid-state magnetic data, Mössbauer spectroscopy, and X-ray diffraction demonstrated that these compounds are best described as having an intermediate spin ferric center ($S_{Fe} = 3/2$) antiferromagnetically coupled to a chelate radical anion, [^{iPr}PDI]$^{1-}$, with a traditional [NR]$^{2-}$ fragment, producing an overall $S = 1$ ground state. The solid-state structures also revealed distorted four-coordinate geometries where the Fe=NR vector was nearly linear but significantly lifted from the idealized iron-chelate plane. The Fe−N_{imide} bond lengths of 1.7048(16) (Ar = 2,6-^{i}Pr$_2$-C_6H_3) and 1.7165(15) Å (Ar = 2,4,6-Me$_3$-C_6H_2) are some of the longest known for terminal iron imides, consistent with an iron−nitrogen bond order less than three.[13] In three cases, addition of dihydrogen to the (^{iPr}PDI)FeNAr compounds (Ar = 2,6-^{i}Pr$_2$-C_6H_3; 2,6-Et$_2$-C_6H_3; 2,5-^{t}Bu$_2$-C_6H_3) resulted in complete hydrogenation of the iron−nitrogen bond and liberation of the corresponding free aniline. Catalytic hydrogenation of the aryl azides to the anilines was observed in the presence of (^{iPr}PDI)Fe(N_2)$_2$ (Scheme 1).[26] This reactivity is inspiring for hypothetical cycles involving homogeneous N_2 hydrogenation[27] and suggests that, if sufficient imido character can be imparted to an iron dinitrogen complex, release of hydrogenated products may indeed be plausible.

In this context, efforts have also been devoted toward the preparation of the bis(imino)pyridine iron parent imido derivative, [(^{iPr}PDI)Fe=NH], by treatment of (^{iPr}PDI)Fe(N_2)$_2$ with the [NH] group transfer agent, Hdbabh (dbabh =2,3:5,6-dibenzo-7-azabicyclo[2.2.1]hepta-2,5-diene).[28] Instead of the desired iron imido product, a 3:1 mixture of the iron amide and iron ammonia compounds, (^{iPr}PDI)Fe(dbabh) and (^{iPr}PDI)FeNH_3, respectively, was isolated (Scheme 2). Deuterium-labeling studies were consistent with initial [NH] group transfer to form the desired parent iron imide, [(^{iPr}PDI)Fe=NH], followed by N−H activation of the remaining Hdbabh to yield the observed products.

The structural distortions, electronic structure, and hydrogenation activity of the (^{iPr}PDI)FeNAr compounds and the proposed N−H bond activation chemistry of the putative parent imide, (^{iPr}PDI)FeNH, prompted exploration of other bis(imino)pyridine iron imido complexes with different imido nitrogen substituents. By manipulating both the steric and electronic properties of this group, we sought to determine the origin and importance of the deviation of the [NR] ligand from planarity and the impact of this distortion on the electronic structure and ultimately the reactivity of the molecule. Similar to the bis(imino)pyridine chelate, imido ligands are also redox-active[19,20] rendering overall electronic structure determination of (^{iPr}PDI)FeNR compounds challenging. Here we describe the synthesis and spectroscopic characterization of three new bis(imino)pyridine iron imido compounds bearing *N*-alkyl imido substituents and establish spin crossover between $S = 0$ and $S = 1$ states. This behavior is distinct from the *N*-arylated variants and highlights the redox flexibility of both the bis(imino)pyridine and the imido fragments.

RESULTS AND DISCUSSION

Synthesis and Characterization of Bis(imino)pyridine Iron *N*-Alkyl Imido Complexes. The synthetic method used to prepare the bis(imino)pyridine iron *N*-aryl imido compounds[26] was extended to three new *N*-alkyl derivatives. Slow addition of a pentane solution of either ^{1}AdN$_3$, ^{2}AdN$_3$, or ^{Cy}OctN$_3$ (^{1}Ad = 1-adamantyl; ^{2}Ad = 2-adamantyl; ^{Cy}Oct = cyclooctyl) to a pentane solution of

Scheme 2. Preparation of Transient [(^{iPr}PDI)FeNH] by [NH] Group Transfer

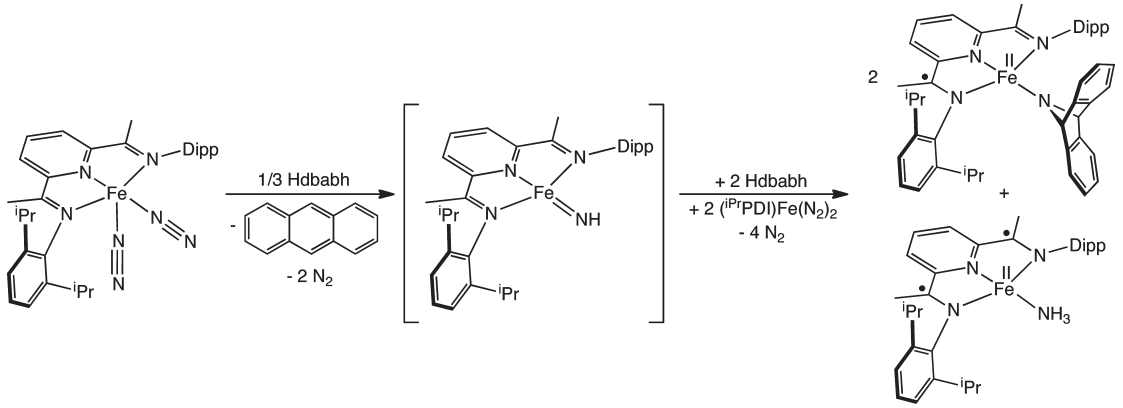

(^{iPr}PDI)Fe(N_2)$_2$ resulted in rapid effervescence of nitrogen gas and furnished the desired iron *N*-alkyl imide complexes, (^{iPr}PDI)FeN^{1}Ad and (^{iPr}PDI)FeN^{Cy}Oct, as dark purple crystals in 60 and 86% yields, respectively, and (^{iPr}PDI)FeN^{2}Ad as black crystals in 73% yield following recrystallization (eq 1). Slow addition of the azide is required to avoid formation of iron tetrazole compounds, (^{iPr}PDI)Fe[(R)N_4(R)],[29] the synthesis and full characterization of which will be reported elsewhere.[30] We note that until the data for the electronic structures of the compounds are presented, the molecules will be drawn with the bis(imino)pyridine ligand in its neutral form.

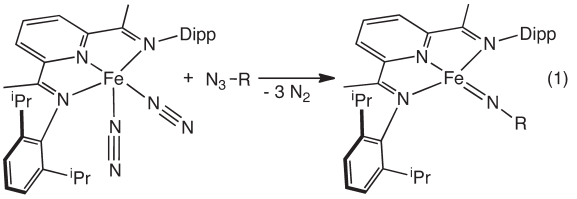

(^{iPr}PDI)Fe(N_2)$_2$

(^{iPr}PDI)FeN^{1}Ad: R = 1-Adamantyl (60 %)
(^{iPr}PDI)FeN^{2}Ad: R = 2-Adamantyl (73 %)
(^{iPr}PDI)FeN^{Cy}Oct: R = cyclooctyl (86 %)

The two isomeric iron imides, (^{iPr}PDI)FeN^{1}Ad and (^{iPr}PDI)FeN^{2}Ad, exhibit different NMR spectral features in benzene-d_6 solution at 23 °C. In contrast to the previously reported *N*-aryl substituted bis(imino)pyridine iron imido compounds with $S = 1$ ground states,[26] (^{iPr}PDI)FeN^{1}Ad exhibits sharp and readily assignable ^{1}H and ^{13}C NMR spectra with observable *J* couplings at 23 °C, suggestive of an $S = 0$ ground state. Similar spectra are observed for (^{iPr}PDI)FeN^{Cy}Oct. Both compounds exhibit the number of peaks consistent with C_{2v} symmetric molecules in solution. Despite the appearance of $S = 0$ ground states, widely dispersed chemical shifts, especially for the in-plane chelate hydrogens, were observed (Figure S1, Supporting Information [SI]). For example, the imine methyl groups appear at −15.25 and −16.36 ppm for (^{iPr}PDI)FeN^{1}Ad and (^{iPr}PDI)FeN^{Cy}Oct, respectively. Likewise, the *meta*- and *para*-pyridine hydrogens of (^{iPr}PDI)FeN^{1}Ad were located at 16.41 and 22.30 ppm. For (^{iPr}PDI)FeN^{Cy}Oct, these hydrogens were located at 18.02 and 20.64 ppm, respectively.

By contrast, the benzene-d_6 ^{1}H NMR spectrum of (^{iPr}PDI)FeN^{2}Ad at 23 °C is reminiscent of the $S = 1$ (^{iPr}PDI)FeN*Ar* compounds with resonances located over a 200 ppm chemical shift window. For example, the imine methyl group was located at −121 ppm and the most downfield resonance, either the *p*-pyridine or a 2-adamantyl hydrogen, appears at 94.01 ppm. A benzene-d_6 solution magnetic moment of 2.8 μ_B was measured at 23 °C, consistent with an $S = 1$ state at this temperature.

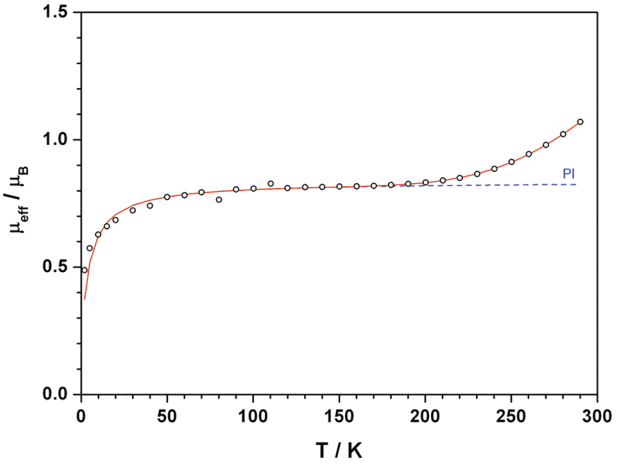

Figure 1. Variable-temperature SQUID magnetization data for (^{iPr}PDI)FeN^{1}Ad. Experimental data are represented by open circles; data are corrected for underlying diamagnetism. The simulation (red line) is a superposition of a paramagnetic impurity with Curie−Weiss behavior (8% $S = 1$, $\Theta_W = -8$ K, blue line) and an $S = 0$ to $S = 1$ phase transition, for which the high-spin fraction is given by $x = 1/[1 + \exp\{(n\Delta H/R)(1/T - 1/T_c)\}]$ according to Sorai's domain model,[32,33] with a transition temperature $T_c = 482$ K and an enthalpy term $n\Delta H = 1442$ cm^{-1} for domain size *n*, which determines the width of the transition.

In order to determine whether the unusual shifts are due to thermal population of a low-lying triplet ($S = 1$) excited state, a phenomenon observed by Budzelaar and co-workers in related bis(imino)pyridine cobalt alkyl compounds,[31] variable temperature NMR data in toluene-d_8 solutions were collected for (^{iPr}PDI)FeN^{1}Ad. Cooling the sample resulted in a contraction of the chemical shift dispersion observed for the compound (Figure S2, SI), thereby ruling out temperature-independent paramagnetism.[24] For example, the resonance for the imine methyl group shifts from −15.25 ppm at 23 °C to 0.06 ppm at −80 °C, the lowest temperature experimentally accessible. Likewise, the *p*-pyridine resonance moves upfield from 22.30 ppm at 23 °C to 9.27 ppm at −80 °C.

dx.doi.org/10.1021/ja205736m |*J. Am. Chem. Soc.* 2011, 133, 17353–17369

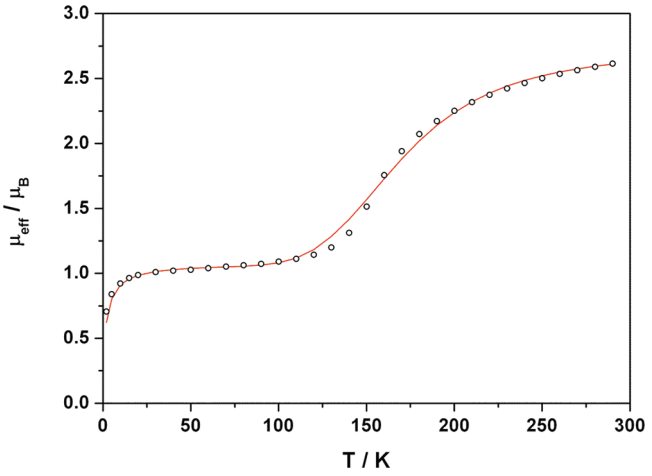

Figure 2. Variable-temperature SQUID magnetization data for (^{iPr}PDI)FeN^{2}Ad. Experimental data are represented by open circles; data are corrected for underlying diamagnetism. The simulation (red line) is an $S = 0$ to $S = 1$ phase transition, for which the high-spin fraction is given by $x = 1/[1 + \exp\{(n\Delta H/R)(1/T - 1/T_c)\}]$ according to Sorai's domain model,[32,33] with a transition temperature T_c = 185 K and an enthalpy term $n\Delta H$ = 738 cm^{-1} for domain size n, which determines the width of the transition.

The unusual NMR shifts and behavior of the three new iron imide compounds prompted a more thorough investigation of their magnetic properties. The two isomeric compounds, (^{iPr}PDI)FeN^{1}Ad and (^{iPr}PDI)FeN^{2}Ad, were selected as representative examples. The effective magnetic moment was measured for a polycrystalline sample of (^{iPr}PDI)FeN^{1}Ad between 2 and 300 K by SQUID magnetometry. The data (Figure 1, open circles) exhibit a steep increase with increasing temperature, followed by a plateau at 0.8 μ_B and a second steep increase in effective magnetic moment. The plateau is higher than the magnetic susceptibility value expected for an $S = 0$ state; however, this low-temperature region was successfully modeled using 8% of an $S = 1$ paramagnetic compound (Figure 1, blue line). This component was also observed by Mössbauer spectroscopy (*vide infra*) and is derived from intramolecular C−H bond activation of the bis(imino)pyridine ligand by (^{iPr}PDI)FeN^{1}Ad, the details of which will be presented elsewhere.[30] The increase of $\mu_{eff}(T)$ above 150 K, however, could *not* be reasonably modeled using Boltzmann population of a low-lying triplet state; the onset temperature and the slope of the curve would not be consistent (Figure S3, SI).

Instead, the high temperature increase is consistent with spin crossover (SCO) from an $S = 0$ to an $S = 1$ ground state, although complete transition to the $S = 1$ state was not observed at the temperatures studied. The data were fit using the domain model proposed by Sorai and Seki for a SCO transition[32,33] with a transition temperature of 483 K; thus, observation of a complete transition is not expected (the high-spin fraction at 300 K is 6.8%). In addition, the change in chemical shift observed for the methyl backbone resonance of (^{iPr}PDI)FeN^{1}Ad by variable-temperature ^{1}H NMR could be fit using a similar SCO model for independent molecules in solution, yielding a somewhat higher transition temperature (865 K) than the solid-state magnetization data (Figure S4, SI). Spin crossover behavior is commonly observed for iron(II) and iron(III) compounds, especially for complexes where strong field ligands such as 1,10-phenanthroline or bipyridine are combined with ligands of intermediate field strength, such as thiocyanate (NCS^-).[34] Spin crossover behavior is also well-documented for iron complexes with terdentate ligands, such as the terpyridine derivatives 2,4-bis-(2-pyridyl)thiazole and 2-(2-pyridylamino)-4-(2-pyridyl)thiazole.[35]

The effective magnetic moment was also measured for a polycrystalline sample of (^{iPr}PDI)FeN^{2}Ad between 2 and 300 K (Figure 2). Although the NMR spectra for (^{iPr}PDI)FeN^{2}Ad at 23 °C are similar to those observed for the aryl-substituted imido complexes at the same temperature, the solid-state magnetic data are markedly different from the simple $S = 1$ behavior observed for (^{iPr}PDI)FeN*Ar*. Analogous to (^{iPr}PDI)FeN^{1}Ad, the solid-state magnetic data demonstrate spin crossover from an $S = 0$ to an $S = 1$ state. However, for (^{iPr}PDI)FeN^{2}Ad, the data exhibit a more pronounced spin transition and demonstrate that the $S = 1$ state is dominant at room temperature. This spin state is consistent with the NMR data where paramagnetically broadened and shifted resonances are observed at 23 °C. As with (^{iPr}PDI)FeN^{1}Ad, the low temperature plateau is higher than expected for an $S = 0$ state. However, in the case of (^{iPr}PDI)FeN^{2}Ad this results from the presence of some fraction of the high-spin species even at low temperatures. This was confirmed by Mössbauer spectroscopy and will be discussed in a later section of the article.

X-ray Crystallographic Studies. The solid-state structures of all three bis(imino)pyridine iron imides prepared in this work were determined by single-crystal X-ray diffraction. Representations of the molecules are presented in Figures 3−5 and selected metrical parameters are presented in Tables 1 and 2. Also included in Table 1 are the corresponding distances and angles for the previously structurally characterized $S = 1$ bis(imino)pyridine iron *N*-aryl substituted imido complexes, (^{iPr}PDI)FeNDipp and (^{iPr}PDI)FeNMes (Dipp =2,6-^{i}Pr$_2$-C$_6$H$_3$; Mes =2,4,6-Me$_3$-C$_6$H$_2$).[26]

Consistent with the idealized C_{2v} symmetry observed in solution by NMR spectroscopy, the solid-state structure of (^{iPr}PDI)FeN^{1}Ad has a crystallographically imposed mirror plane that contains the N(2)−Fe(1)−N(3) plane and renders the two halves of the molecule equivalent. As is typical in compounds of this type, the aryl groups are oriented such that the isopropyl substituents are above and below the metal−chelate plane. The iron imide group is slightly lifted from the idealized square plane of the molecule with an N_{py}−Fe−N_{imide} angle of 168.10(8)°. This distortion is significantly smaller than those observed with the *N*-aryl substituted imides, (^{iPr}PDI)FeN*Ar*, where N_{py}−Fe−N_{imide} angles of 138.79(7)° (*Ar* = Dipp) and 154.75(7)° (*Ar* = Mes) were observed. In (^{iPr}PDI)FeN^{1}Ad, the iron imide is slightly bent with an Fe−N_{imide}−C_{imide} angle of 159.87(15)°.

The solid state structure of (^{iPr}PDI)FeN^{Cy}Oct was also determined by single crystal X-ray diffraction. Only small, weakly diffracting crystals were obtained and as a result the data were collected at 293 K using synchrotron (λ = 0.9782 Å) radiation. The overall molecular geometry of the compound is similar to (^{iPr}PDI)FeN^{1}Ad (Figure 4). Two molecules are present in the unit cell, and metrical parameters for both are presented in Table 1. Given the similarity between the data, only values from one will be cited in the subsequent discussion. An idealized (but not crystallographically imposed) C_{2v} geometry is observed with the orientation of the cyclooctyl substituent responsible for the descent in symmetry. The iron imide group is the most planar observed in the bis(imino)pyridine series of compounds with an N_{py}−Fe−N_{imide} angle of 175.14(16)°. As with other iron imides reported in Table 1, a slight bend is observed at the imide nitrogen with an Fe−N_{imide}−C_{imide} angle of 160.9(3)°.

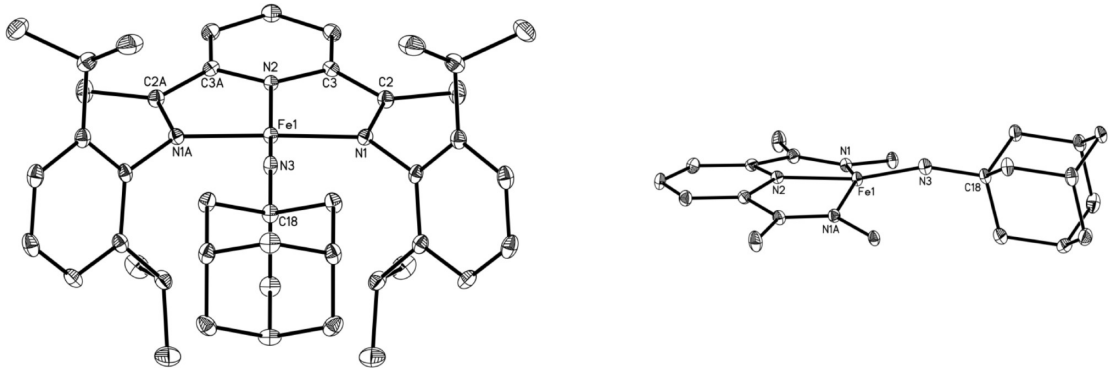

Figure 3. Solid-state structure of (^{iPr}PDI)FeN^{1}Ad (left) and core of the molecule (right) at 30% probability ellipsoids. Hydrogen atoms omitted for clarity.

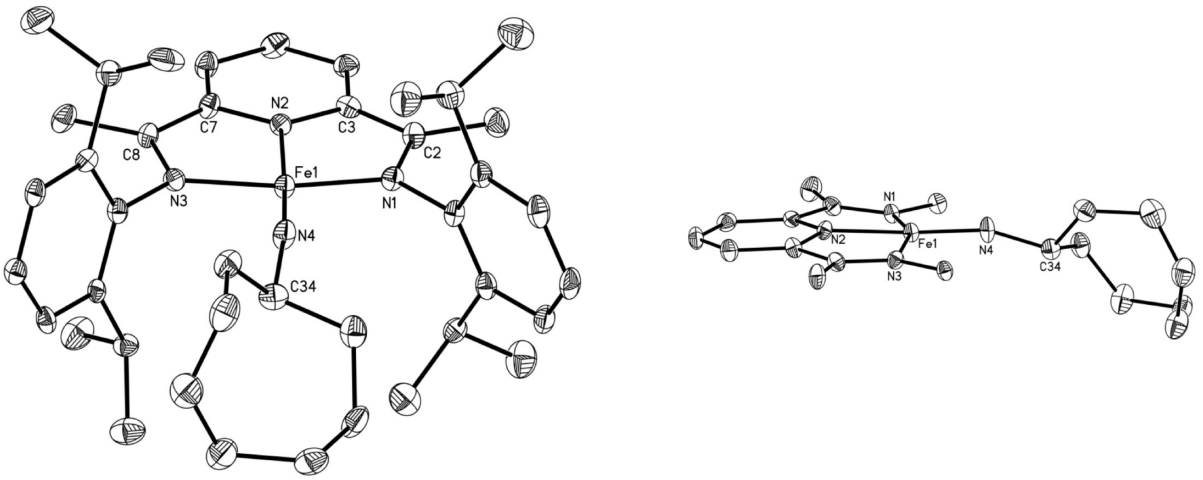

Figure 4. Solid-state structure of (^{iPr}PDI)FeN^{Cy}Oct (left) and core of the molecule (right) at 30% probability ellipsoids. Hydrogen atoms omitted for clarity.

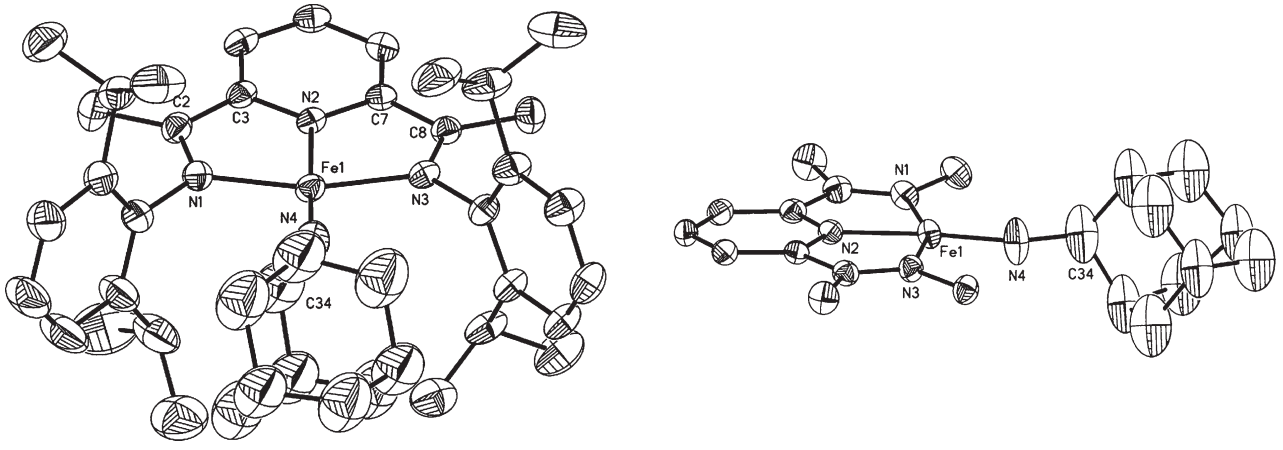

Figure 5. Solid-state structure of (^{iPr}PDI)FeN^{2}Ad (left) and core of the molecule (right) at 30% probability ellipsoids. Hydrogen atoms omitted for clarity. Data collected at 253 K.

In both (^{iPr}PDI)FeN^{1}Ad and (^{iPr}PDI)FeN^{Cy}Oct, the Fe−N$_{imide}$ distances of 1.6481(15) and 1.648(3) Å are statistically indistinguishable from each other but are significantly shorter than the Fe−N$_{imide}$ bond lengths of 1.705(2) (*Ar* = Dipp) and 1.717(2) Å (*Ar* = Mes) reported for the (^{iPr}PDI)FeN*Ar* compounds. The shorter Fe−N$_{imide}$ bonds in the *N*-alkyl substituted compounds are in the range of 1.625(4) to 1.6578(2) Å typically observed in neutral, monomeric iron derivatives with terminal iron imide ligands.[1] The metrical parameters of the bis(imino)pyridine chelates in both (^{iPr}PDI)FeN^{1}Ad and (^{iPr}PDI)FeN^{Cy}Oct are within

dx.doi.org/10.1021/ja205736m |*J. Am. Chem. Soc.* 2011, 133, 17353–17369

Table 1. Selected Bond Distances (Å) and Angles (deg) for (^{iPr}PDI)FeN^{1}Ad, (^{iPr}PDI)FeN^{Cy}Oct, and (^{iPr}PDI)FeN*Ar*[a]

	(^{iPr}PDI)FeN^{1}Ad	(^{iPr}PDI)FeN^{Cy}Oct	(^{iPr}PDI)FeN^{Cy}Oct	(^{iPr}PDI)FeNDipp	(^{iPr}PDI)FeNMes
Fe−N_{imide}	1.648(2)	1.648(3)	1.658(3)	1.705(2)	1.717(1)
Fe−N_{py}	1.895(2)	1.870(3)	1.884(3)	1.840(2)	1.872(1)
Fe−N_{imine}	1.933(1)	1.901(3)	1.917(3)	2.034(2)	2.011(1)
		1.908(3)	1.917(3)	1.987(2)	1.979(1)
N_{imine}−C_{imine}	1.340(2)	1.345(5)	1.347(5)	1.320(2)	1.321(2)
		1.355(5)	1.347(5)	1.331(2)	1.334(2)
C_{imine}−C_{ipso}	1.418(2)	1.405(5)	1.409(5)	1.437(3)	1.436(2)
		1.406(5)	1.413(6)	1.431(3)	1.426(2)
N_{py}−Fe−N_{imide}	168.10(8)	175.14(16)	172.78(15)	138.79(7)	154.75(7)
Fe−N_{imide}−C_{ipso}	159.87(15)	160.9(3)	157.7(4))	165.68(15)	159.00(13)

[a] Data for the (^{iPr}PDI)FeN*Ar* compounds taken from reference 26.

the range established for two-electron reduction (Table 1).[24,25] Notably, the distortions to the chelate are more pronounced in these compounds than those observed for the (^{iPr}PDI)FeN*Ar* derivatives where one-electron bis(imino)pyridine reduction was assigned.[26] Thus, the position of the terminal iron imide influences the degree of bis(imino)pyridine ligand reduction and hence electronic configuration at the metal.

X-ray quality crystals of (^{iPr}PDI)FeN^{2}Ad were obtained by cooling a concentrated pentane solution of the compound to −35 °C. Because of the spin crossover behavior of the compound, data were collected at three temperatures: 100, 220, and 253 K. These temperatures were selected to obtain metrical data on the low- and high-spin forms as well as at an intermediate temperature. Unfortunately, cooling the sample to temperatures below 220 K consistently results in cracking of the crystal. Accordingly, the data at 100 K are of relatively poor quality. For example, high-quality data were collected at 253 K, then cooling the sample resulted in the presence of multiple crystallographic domains and weakening of the diffraction strength. A representation of the solid-state structure determined at 253 K is presented in Figure 5. Selected metrical parameters from all three data sets are presented in Table 2.

The solid-state structure (Figure 5) establishes a C_{2v} symmetric molecule with idealized planar geometry with the sum of the angles around iron equal to 360.08(9)°. The N_{py}−Fe−N_{imide} angle of 176.28(15)° is nearly identical to that observed for (^{iPr}PDI)FeN^{Cy}Oct, indicating that the imide substituent is not significantly lifted out of the idealized plane of the chelate (Table 2). It should be noted that there is disorder and thermal motion in the adamantyl group, resulting in elongation of the N(4) ellipsoids. While this possibly indicates a deviation from planarity, this distortion is small and not on the order of the deviation seen with the aryl-substituted iron imides.

The Fe−N_{imide} bond length of 1.680(3) Å observed for (^{iPr}PDI)FeN^{2}Ad is slightly longer than the Fe−N_{imide} distances for (^{iPr}PDI)FeN^{1}Ad and (^{iPr}PDI)FeN^{Cy}Oct. The Fe−N_{imide} distance for (^{iPr}PDI)FeN^{2}Ad is also shorter than the Fe−N_{imide} distances for (^{iPr}PDI)FeNDipp and (^{iPr}PDI)FeNMes. Consistent with all other structurally characterized bis(imino)pyridine iron imide complexes, a modest bend is observed at the imide nitrogen with an Fe−N_{imide}−C angle of 155.6(4)°. Examination of the metrical parameters of the bis(imino)pyridine chelate establish elongation of the C_{imine}−N_{imine} bonds and contraction of the C_{imine}−C_{ipso} bonds that are consistent with two electron reduction.

Table 2. Selected Bond Distances (Å) and Angles (deg) for (^{iPr}PDI)FeN^{2}Ad at 253 K, 220 K, and 100 K

	(^{iPr}PDI)FeN^{2}Ad (253 K)	(^{iPr}PDI)FeN^{2}Ad (220 K)	(^{iPr}PDI)FeN^{2}Ad (100 K)
Fe−N_{imide}	1.680(3)	1.675(4)	1.666(10)
Fe−N_{py}	1.899(2)	1.898(2)	1.880(9)
Fe−N_{imine}	1.983(2)	1.978(2)	1.971(9)
	1.964(2)	1.960(2)	1.929(9)
N_{imine}−C_{imine}	1.323(4)	1.337(4)	1.367(12)
	1.330(4)	1.339(4)	1.367(14)
C_{imine}−C_{ipso}	1.434(4)	1.434(4)	1.431(13)
	1.415(4)	1.414(4)	1.387(15)
N_{py}−Fe−N_{imide}	176.28(15)	175.64(13)	172.4(4)
Fe−N_{imide}−C_{ipso}	155.6(4)	158.7(4)	155.6(15)

The C_{imine}−N_{imine} bond lengths are elongated to 1.323(4) Å and 1.330(4) Å, while the C_{imine}−C_{ipso} distances are contracted to 1.434(4) Å and 1.415(4) Å. These distortions are similar to those observed with (^{iPr}PDI)FeN^{1}Ad and (^{iPr}PDI)FeN^{Cy}Oct and are diagnostic of two-electron reduction. The Fe−N_{py} distance of 1.899(2) Å and the Fe−N_{imine} distances of 1.983(2) Å and 1.964(2) Å are significantly longer than the iron−ligand distances exhibited by the molecular structures of (^{iPr}PDI)FeN^{1}Ad and (^{iPr}PDI)FeN^{Cy}Oct. As demonstrated by an overlay of the molecular structures of isomeric (^{iPr}PDI)FeN^{1}Ad and (^{iPr}PDI)-FeN^{2}Ad (Figure S5, SI), the imide nitrogen and *N*-adamantyl substituent of (^{iPr}PDI)FeN^{1}Ad are lifted out of the plane of the chelate at an angle of 168.10(8)°, which is significantly larger than the angle of 176.28(15)° observed for (^{iPr}PDI)FeN^{2}Ad. However, the adamantyl groups overlay quite well for both complexes. In addition, the shorter Fe−N_{imide} bond length of 1.6481(15) Å is apparent in (^{iPr}PDI)FeN^{1}Ad.

Mössbauer Spectroscopic Studies. The electronic structures of the bis(imino)pyridine iron imide complexes were also investigated by both zero- and applied-field ^{57}Fe Mössbauer spectroscopies. Representative zero-field spectra for (^{iPr}PDI)FeN^{1}Ad and (^{iPr}PDI)FeN^{Cy}Oct are presented in Figure 6, and the data are summarized in Table 3. The zero-field spectra of (^{iPr}PDI)-FeN^{2}Ad are temperature dependent and are more complex. The discussion of these data will be presented separately.

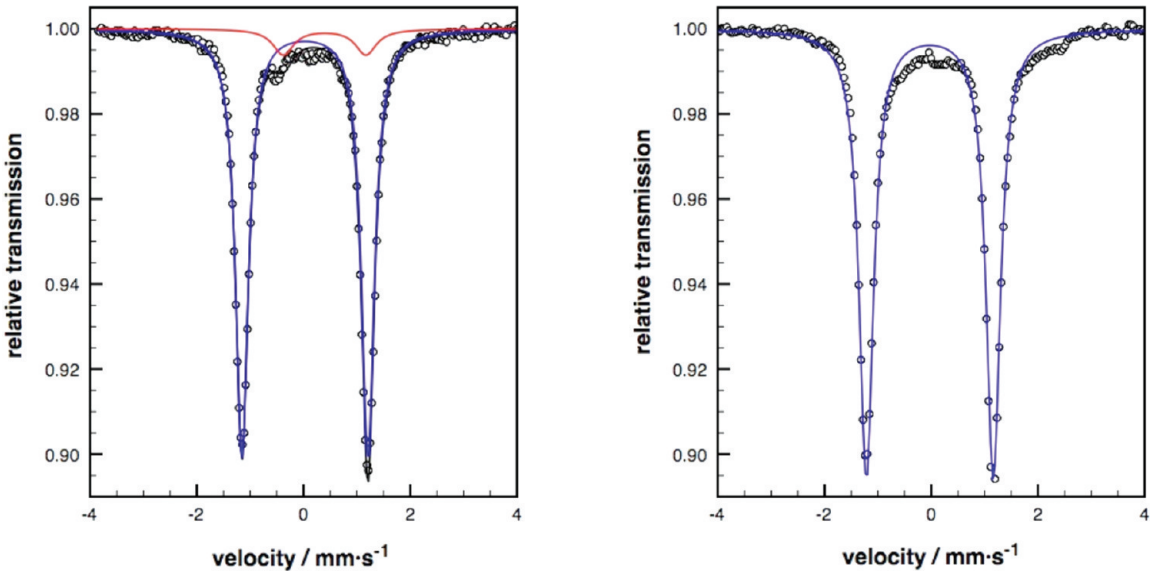

Figure 6. Zero-field ^{57}Fe Mössbauer spectra of (^{iPr}PDI)FeN^{1}Ad (left) and (^{iPr}PDI)FeN^{Cy}Oct (right) recorded at 80 K.

The *N*-alkyl substituted imides, (^{iPr}PDI)FeN^{1}Ad and (^{iPr}PDI)-FeN^{Cy}Oct, have isomer shifts of 0.04 and −0.02 mm·s^{-1}, respectively, significantly lower than the values of 0.30 mm·s^{-1} measured for both (^{iPr}PDI)FeN*Ar* compounds (Table 3).[26] The *N*-alkyl substituted imides, (^{iPr}PDI)FeN^{1}Ad and (^{iPr}PDI)-FeN^{Cy}Oct also exhibit quadrupole splittings of |2.38| mm·s^{-1}, larger than the absolute values of 1.08 and 1.34 mm·s^{-1} determined for (^{iPr}PDI)FeNDipp and (^{iPr}PDI)FeNMes, respectively. Because some degree of spin transition was observed in the SQUID magnetization data, the Mössbauer spectrum of (^{iPr}PDI)-FeN^{1}Ad was also recorded at room temperature (Figure S7, SI). However, there is no observable difference from the 80 K spectrum, as is consistent with the incomplete spin crossover and the resulting small amount of the high-spin fraction at 298 K.

Because complete spin crossover behavior for (^{iPr}PDI)-FeN^{2}Ad was established by SQUID magnetometry, zero-field ^{57}Fe Mössbauer spectra were recorded over a range of temperatures (Figure 7). The spectrum obtained at 15 K exhibits a single Mössbauer doublet with an isomer shift of 0.01 mm·s^{-1} and a quadrupole splitting of |2.26| mm·s^{-1}, parameters that are similar to the other alkyl iron imides (Table 3). However, upon warming the sample to 80 K, a second quadrupole doublet was observed that increased in intensity with additional warming. The intensity of the doublet observed at 15 K decreased until it was no longer observed at 200 K (Figure 7). The parameters of the second quadrupole doublet (δ = 0.19 mm·s^{-1} and ΔE_Q = 0.75 mm·s^{-1}) are significantly different than the parameters of the doublet observed at 15 K. Cooling the sample again to 15 K regenerated the initial spectrum observed at that temperature, indicating the spin crossover behavior is reversible. A small decrease in magnitude for both the isomer shift and the quadrupole splitting of the S = 1 doublet was observed with increasing temperature. Temperature-dependent Mössbauer parameters for a given doublet have been observed due to population of close-lying excited states, where relaxation on the experimental time scale is fast compared to the excited-state lifetime such that the observed doublet represents an average of the ground state and any populated excited states.[35] Generally the isomer shift and quadrupole splitting decrease with increasing temperature, as is observed for (^{iPr}PDI)FeN^{2}Ad.

Table 3. ^{57}Fe Mössbauer parameters of bis(imino)pyridine iron imide compounds recorded at 80 K

compound	δ (mm·s^{-1})	ΔE_Q (mm·s^{-1})
(^{iPr}PDI)FeN^{1}Ad	0.04	−2.38
(^{iPr}PDI)FeN^{2}Ad	0.01	−2.26
(^{iPr}PDI)FeN^{Cy}Oct	−0.02	2.38[c]
(^{iPr}PDI)FeNDipp[a]	0.30	+1.08
(^{iPr}PDI)FeNMes[b]	0.30	1.34[c]

[a] Data taken from reference 26. [b] See Figure S6, SI. [c] Sign not determined.

The presence of two temperature-dependent species in the zero-field Mössbauer spectrum is consistent with spin crossover behavior, and the relative amounts of the two iron species at a given temperature are approximately consistent with the variable-temperature magnetic data (Figure 2). Using the concentrations of each species observed at each temperature by Mössbauer spectroscopy, a van't Hoff plot was constructed (Figure S8, SI). The fit of the data yielded the following thermodynamic parameters, $\Delta H°$ = 4.10(25) kJ·mol^{-1} and $\Delta S°$ = 31.6(1.9) J·K^{-1}·mol^{-1}, consistent with a low-spin compound converting to a higher-spin species at higher temperatures. The spin transition was also observed visually, with a color change from black to purple occurring upon cooling a benzene solution to 77 K.[36]

The van't Hoff relationship established for the spin transition in (^{iPr}PDI)FeN^{2}Ad by variable temperature Mössbauer spectroscopy and the fitting of the NMR data for (^{iPr}PDI)FeN^{1}Ad allow comparison of the relative enthalpies for conversion from the low spin species to the high spin species for each compound. For (^{iPr}PDI)FeN^{2}Ad, a value of ΔH = 342 cm^{-1} was obtained while for the isomeric (^{iPr}PDI)FeN^{1}Ad derivative a value ΔH = 1083 cm^{-1} was determined.

Applied-field Mössbauer spectra were collected on examples of an *N*-alkyl and an *N*-aryl substituted bis(imino)pyridine imide

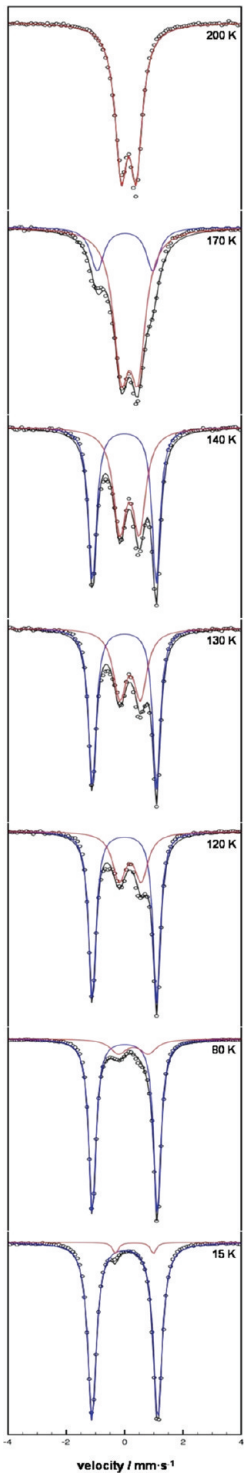

Figure 7. Variable temperature zero-field ^{57}Fe Mössbauer spectra of (^{iPr}PDI)FeN^{2}Ad.

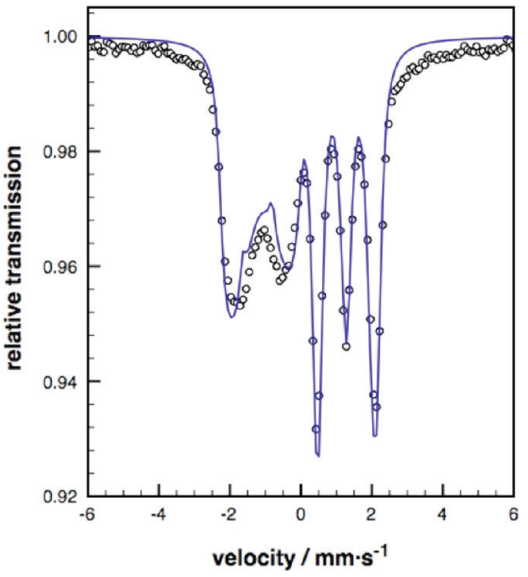

Figure 8. Applied field Mössbauer spectrum of (^{iPr}PDI)FeN^{1}Ad recorded at 7 T and 4.2 K.

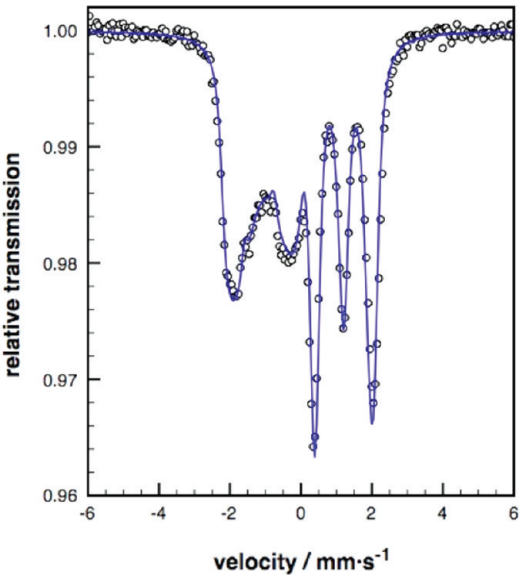

Figure 9. Applied field Mössbauer spectrum of (^{iPr}PDI)FeN^{2}Ad recorded at 7 T and 4.2 K.

to gain additional insight into the electronic structure differences in the two classes of compounds. (^{iPr}PDI)FeN^{1}Ad was chosen as a representative example of an *N*-alkyl substituted imido complex while (^{iPr}PDI)FeNDipp was chosen as a representative example for the *N*-aryl class of imides. The applied-field spectrum of (^{iPr}PDI)FeN^{2}Ad was also obtained to examine the $S = 0$ state observed at low temperature. The experimental data for (^{iPr}PDI)FeN^{1}Ad, (^{iPr}PDI)FeN^{2}Ad, and (^{iPr}PDI)FeNDipp are presented in Figures 8, 9 and 10, respectively. The data for (^{iPr}PDI)FeN^{1}Ad and (^{iPr}PDI)FeN^{2}Ad were recorded at 7 T, both at 4.2 and 15 K. The data for (^{iPr}PDI)FeN^{1}Ad were simulated using the δ and ΔE_Q parameters from the zero-field measurements and indicate an $S = 0$ ground state for the molecule. This is also supported by the observation that there is no discernible difference between the applied-field spectra at different temperatures, as is expected with a diamagnetic ground state. From the fit of the data, the sign and magnitude of the quadrupole splitting was determined to be -2.38 mm·s^{-1} with an asymmetry parameter $\eta = 0.28$. Because an identical value of $|2.38|$ mm·s^{-1} was measured for (^{iPr}PDI)FeN^{Cy}Oct, and the two compounds otherwise have nearly identical spectroscopic

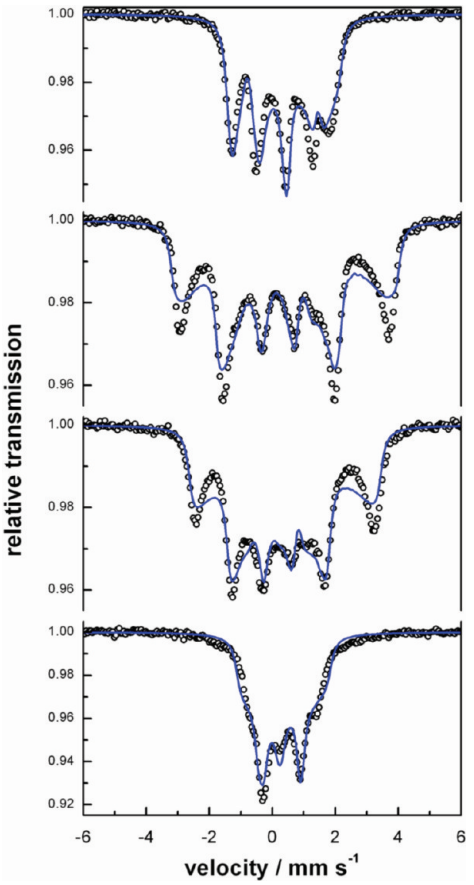

Figure 10. Applied field Mössbauer spectra of (^{iPr}PDI)FeNDipp recorded at 1 T, 4.2 K (bottom); 4 T, 4.2 K; 7 T, 4.2 K; 7 T, 60 K (top).

parameters, it is almost certain that the sign of ΔE_Q for (^{iPr}PDI)-FeN^{Cy}Oct is also negative.

The data for (^{iPr}PDI)FeN^{2}Ad were also simulated using the δ and ΔE_Q parameters from the zero-field measurement. Similar to (^{iPr}PDI)FeN^{1}Ad, a quadrupole splitting of -2.26 mm·s^{-1} and an asymmetry parameter η = 0.26 were determined for (^{iPr}PDI)FeN^{2}Ad from the fit of the applied field data. The data were successfully fit using an S = 0 model, and there was no evident change in the applied-field spectra at different temperatures. This indicates an S = 0 ground state for (^{iPr}PDI)FeN^{2}Ad at the temperatures measured (15 K and below), consistent with the solid-state magnetic data (Figure 2).

Applied-field measurements were also carried out on (^{iPr}PDI)FeNDipp at 4.2 K and at magnetic fields of 1 T, 4 T, 7 T, as well as at 60 K with a magnetic field of 7 T. The data were simulated using the δ and ΔE_Q parameters obtained from the zero-field spectrum and an S = 1 spin state for the molecule (Figure 10). The fit of the data for (^{iPr}PDI)FeNDipp established a positive quadrupole splitting of +1.08 mm·s^{-1}. While the applied field measurement on (^{iPr}PDI)FeNMes was not carried out, the similarity of this compound to (^{iPr}PDI)FeNDipp suggests that the sign of $|1.34|$ for ΔE_Q obtained from the zero-field measurement is also positive. In addition, the fit of the data yielded hyperfine coupling constants of $A_{xx}/g_N\beta_N$ = -81.95, $A_{yy}/g_N\beta_N$ = -8.69, and $A_{zz}/g_N\beta_N$ = 145.60 kG, and an asymmetry parameter, η, of 0.39. The obtained A values indicate an internal magnetic field around the iron nucleus where the majority of spin is on the metal center, consistent with an

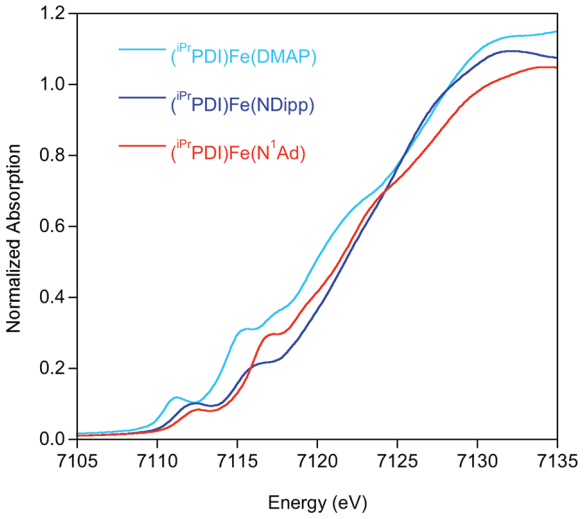

Figure 11. Comparison of the normalized Fe K-edge XAS spectra for (^{iPr}PDI)Fe(DMAP), (^{iPr}PDI)FeNDipp, and (^{iPr}PDI)FeN^{1}Ad. Data collected at 10 K.

intermediate spin iron(III) assignment.[26] In addition, the fit of the data produced an Euler angle, β, of 49.34° where the β angle is defined as the difference between the magnetic quantization axis (z with respect to the orbitals in a crystal field picture with d_{z^2} along the spin axis) and the main component, V_{max}, of the electric field gradient tensor. This misalignment of the principal coordinate systems for the magnetic hyperfine tensor and the electric field gradient suggests that these two phenomena are dominated by different interactions, which may be correlated to the distorted geometry of the molecule. Note that the angle β can be related to the angle Θ ($\beta \approx 90 - \Theta$), which describes the bending of the imide ligand with respect to the (PDI)Fe plane. A more detailed analysis will be presented in Computational Studies.

X-ray Absorption Spectroscopic Studies. To gain additional insight into the iron oxidation states in each class of iron imide, two representative examples, (^{iPr}PDI)FeNDipp and (^{iPr}PDI)-FeN^{1}Ad, were studied by X-ray absorption spectroscopy. Also included in the study is (^{iPr}PDI)Fe(DMAP), an established iron(II) compound with a dianionic bis(imino)pyridine chelate.[26] A comparison of the normalized Fe K-edge XAS spectra for (^{iPr}PDI)-Fe(DMAP), (^{iPr}PDI)FeNDipp, and (^{iPr}PDI)FeN^{1}Ad is shown in Figure 11. The 1s to 3d pre-edge features appear at 7111.2, 7112.3, and 7112.4 eV for (^{iPr}PDI)Fe(DMAP), (^{iPr}PDI)FeNDipp, and (^{iPr}PDI)FeN^{1}Ad, respectively. This is consistent with an Fe(II) assignment for (^{iPr}PDI)Fe(DMAP)[24] and an Fe(III) assignment for (^{iPr}PDI)FeNDipp and (^{iPr}PDI)FeN^{1}Ad. Similar shifts are observed in the rising edge inflection points, again indicating that an overall ferric oxidation state assignment is most appropriate for (^{iPr}PDI)FeN^{1}Ad. Additional features are present at ~7115–7117 eV, which are tentatively attributed to Fe 1s to PDI ligand π^* transitions. The scans were monitored for photoreduction throughout the course of data collection, and no evidence for beam-dependent reduction was observed. A detailed investigation of the energies and intensities of these features and their correlation to the degree of ligand reduction will be the subject of future studies.

Computational Studies. The electronic structures of the bis(imino)pyridine iron imido complexes were also studied with DFT calculations. Unless otherwise noted, geometry optimizations were initiated from the crystallographically determined

structures, and calculations were performed using the ORCA program on the full molecules without truncations. Two examples, (^{iPr}PDI)FeNDipp and (^{iPr}PDI)FeN^{1}Ad, were chosen as representative for the two distinct classes of imides. Both compounds were structurally characterized and studied by an array of spectroscopic techniques providing numerous experimental benchmarks against which to calibrate the computational results. Recall, a valid computational description must account for the following experimental differences (^{iPr}PDI)FeNDipp and the alkyl-substituted imides, (^{iPr}PDI)FeN^{1}Ad, respectively:

(i) $S = 1$ and $S = 0$ ground states at low temperature
(ii) $[PDI]^{-}$ versus $[PDI]^{2-}$ chelate reduction
(iii) bent versus linear $N_{py}-Fe-N_{imide}$ angle
(iv) long (1.705(2) Å) versus short (1.648(2) Å) $Fe-N_{imide}$ bonds
(v) high ($\delta = 0.30$ mm·s^{-1}) versus low ($\delta = 0.04$ mm·s^{-1}) Mössbauer isomer shifts and quadrupole splitting (ΔE_Q) of opposite sign
(vi) similar Fe K-edge spectra, including pre-edge energies
(vii) ultimately electronic structure descriptions of both the low- and high-spin states of the SCO alkyl-substituted imides

In our initial communication, the electronic structure of the aryl-substitued iron imido complex, (^{iPr}PDI)FeNDipp, was assigned solely on the basis of the experimental data as an intermediate spin ferric compound ($S_{Fe} = 3/2$) antiferromagnetically coupled to a bis(imino)pyridine radical ($S_{PDI} = 1/2$).[26] Performing a geometry optimization on the compound with a triplet ground state using the BP86 functional followed by an unrestricted single-point calculation at the B3LYP level resulted in spontaneous symmetry breaking with three unpaired electrons on the [Fe═N*Ar*] fragment and one electron with opposite spin on the bis(imino)pyridine chelate. This solution is denoted "broken symmetry (3,1)" or "BS(3,1)".[37−39] Examination of the Mulliken spin density plot, presented in Figure 12, reveals a more complex bonding picture. Considerable electron density is located on the imide nitrogen and the 2,6-diisopropylphenyl ring, indicating significant covalency in the $Fe-N_{imide}$ bond. Accordingly, oxidation state assignments based on traditional and overly simplistic formalisms become challenging and possibly meaningless. This situation is reminiscent of $S = 1$ iron(IV) oxo complexes where the covalent interaction between the metal center and the oxo ligand places considerable spin density on the formally O^{2-} ligand.[40,41] In both the iron imido and oxo complexes, it is important to note that the spin density on the imido/oxo ligands is the same sign as the spin on the iron, indicating considerable electron sharing, e.g. covalency, between the metal and multiply bonded ligand. For (^{iPr}PDI)FeNDipp, the DFT studies suggest that even with the ambiguities that arise from covalency, the most reasonable electronic structure description is an intermediate spin ferric compound ($S_{Fe} = 3/2$) antiferromagnetically coupled to a bis(imino)pyridine radical ($S_{PDI} = 1/2$), e.g. (^{iPr}PDI^{1-})Fe^{III} NDipp, as we proposed previously.[26] It is important to note that, in this bonding description and hence iron oxidation state assignment, the imido ligand is considered as a traditional, closed-shell dianionic fragment, $[NAr]^{2-}$.

The structural parameters obtained from the BS(3,1) solution for (^{iPr}PDI)FeNDipp at the BP86 level are in good agreement with the data obtained from X-ray diffraction (Table 4). The computed Mössbauer parameters based on this optimized structure

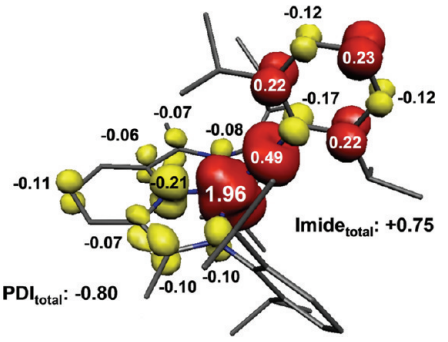

Figure 12. Spin density plot for (^{iPr}PDI)FeNDipp obtained from a Mulliken population analysis.

Table 4. Comparison of Selected Experimental and Computed Bond Distances (Å) and Angles (deg) for (^{iPr}PDI)FeNDipp

	experimental	BP86	B3LYP
$Fe-N_{imide}$	1.705(2)	1.710	1.795
$Fe-N_{py}$	1.840(2)	1.824	2.009
$Fe-N_{imine}$	2.034(2)	1.998	2.481
	1.987(2)	1.977	2.129
$N_{imine}-C_{imine}$	1.320(2)	1.347	1.290
	1.331(2)	1.349	1.330
$C_{imine}-C_{ipso}$	1.437(3)	1.436	1.439
	1.431(3)	1.435	1.482
$N_{py}-Fe-N_{imide}$	138.79(7)	138.58	143.85
$Fe-N_{imide}-C_{ipso}$	165.68(15)	166.60	170.11

are also in good agreement with the experimental values. The calculated isomer shift of 0.22 mm·s^{-1} reproduces the experimental measurement of 0.30 mm·s^{-1} within the accepted error range of 0.10 mm·s^{-1}.[42,43] The small, positive calculated quadrupole splitting of +0.77 mm·s^{-1} is also in excellent agreement with the experimentally observed sign and value of +1.08 mm·s^{-1}. Analysis of the calculated electric field gradient revealed that its orientation is dominated by the short, covalent $Fe-N_{imide}$ bond (Figure 13). The bent (out of the iron chelate plane) coordination of the imido ligand rationalizes the misalignment of the principal coordinate systems of the electric field gradient and the magnetic hyperfine interaction observed in applied field Mössbauer spectroscopy because the latter interaction is most likely dominated by the antiferromagnetic coupling of the iron center with the bis(imino)pyridine radical. The correct alignment of the electric field gradient further substantiates the validity of the calculated electronic structure.

The geometry optimization of (^{iPr}PDI)FeNDipp at B3LYP level of DFT produced a structure that exhibited significant deviations from the crystallographically determined parameters (Table 4). Most significantly, the $Fe-N_{imine}$ bonds are overestimated by more than 0.2 Å, while the $Fe-N_{py}$ bond is elongated by 0.1 Å. Analysis of the computed electronic structure revealed that the overall $S = 1$ ground state arises from a high spin ferrous complex ($S_{Fe} = 2$) antiferromagnetically coupled both to a bis(imino)-pyridine radical anion ($S_{PDI} = 1/2$) and an imidyl radical, $[^{\bullet}NAr]^{1-}$. The computed Mössbauer parameters for this electronic structure ($\delta = 0.64$ mm s^{-1}, $\Delta E_Q = 1.52$ mm s^{-1}), are

dx.doi.org/10.1021/ja205736m |J. Am. Chem. Soc. 2011, 133, 17353–17369

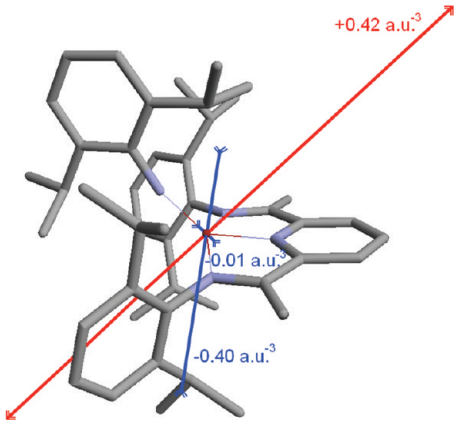

Figure 13. Depiction of the electric field gradient of (^{iPr}PDI)-FeNDipp obtained from B3LYP DFT calculations.

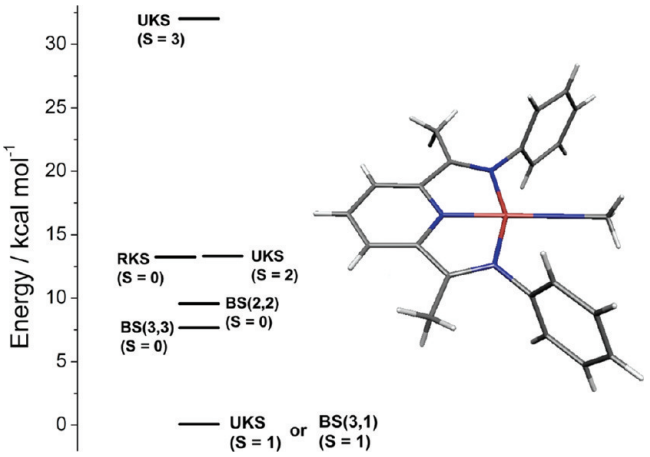

Figure 14. Computed states for (^{H}PDI)FeNMe. All energies are relative to the lowest-lying state (S = 1), and energies were obtained from single-point calculations using the B3LYP functional on the idealized, truncated molecule shown on the right.

typical for a high-spin ferrous complex but disagree with the experimental data. As a result, this electronic structure was discarded. However, this *in silico* experiment demonstrates the sensitivity of the resulting electronic structure description to the computational method and overall molecular geometry. It also highlights that comparison of the computational output with experimentally determined spectroscopic data is crucial for evaluating the validity of the calculations. As will be shown in a subsequent section, this sensitivity is magnified in the essentially planar imides represented by (^{iPr}PDI)FeN^{1}Ad.

The electronic structure of (^{iPr}PDI)FeN^{1}Ad was also explored computationally as a representative alkyl-substituted iron imide that exhibits spin crossover behavior. Recall that both the applied field Mössbauer experiments and magnetic susceptibility measurements established a diamagnetic ground state at cryogenic temperatures. At higher temperatures, however, there is conversion to a triplet ground state, which is further substantiated by the unusual ^{1}H NMR shifts observed at room temperature. The accurate theoretical treatment of SCO complexes is a challenge for modern quantum chemical methods due to the presence of two (or more) states close in energy. Even for simple mononuclear coordination compounds the prediction of the correct ground state by DFT is often challenging.[44] The present case is further complicated by the presence of potentially redox-active bis(imino)pyridine and imido ligands.

As an initial step, a variety of different electronic structures and spin states was investigated. To improve computational expediency, these initial studies were performed without geometry optimization on the simplified model complex, (^{H}PDI)FeNMe, where the 2,6-diisopropyl substituents on the aryl rings were replaced by hydrogen and the N_{imide} adamantyl substituent was replaced by a methyl group. The computational input was also constrained such that the imido fragment was forced into the idealized iron−chelate plane with a perfectly linear Fe−N_{imide}−CH_3 bond and hence overall C_{2v} symmetry. The phenyl rings on the imines were also fixed orthogonally to the metal-chelate plane and the bond distances in the molecule constrained to the values determined by X-ray diffraction. The results obtained from this model system were then used as a benchmark for the full molecule calculations. Computed Mössbauer parameters for various electronic structure descriptions of the model complex, (^{H}PDI)-FeNMe, are reported in Table S1, SI.

At the B3LYP level of theory, several different, energetically plausible spin states were obtained. An ordering of these computed states along with a depiction of the truncated molecule used for these studies is presented in Figure 14. The lowest-energy solution did not correspond to the experimentally determined low temperature S = 0 ground state but rather to a triplet (S = 1) configuration arising from spontaneous symmetry breaking and a BS(3,1) electronic structure description. Despite the difference in geometry (idealized planar versus a lifted FeNR fragment), this electronic structure is nearly identical to the one described for (^{iPr}PDI)FeNDipp, where the iron is best described as intermediate spin ferric (S_{Fe} = 3/2) with strong covalent bonding between the iron center and the [NMe] fragment that results in significant spin delocalization onto the imido ligand. Antiferromagnetic coupling between the half-occupied d_{xz} orbital and the bis(imino)pyridine b_2 SOMO[24] gives rise to the overall S = 1 state. It is important to note that in this solution, the bis(imino)pyridine chelate is in its monoreduced form, e.g. $[PDI]^{1-}$, which is inconsistent with the experimentally obtained crystallographic data for all three alkyl-substituted iron−imido complexes (Tables 1 and 2).

A closed-shell singlet state was obtained using a restricted DFT approach and was found to be 13.2 kcal/mol higher in energy than the BS(3,1) triplet state and is denoted RKS (S = 0) in Figure 14. In this electronic structure, the bis(imino)pyridine ligand is doubly reduced, e.g. $[PDI]^{2-}$ (S_{PDI} = 0), with a doubly occupied b_2 orbital. If the imide ligand is considered in its typical $[NMe]^{2-}$ form then the metal is best described as Fe(IV) with doubly occupied d_{yz} and d_{z^2} orbitals (Figure 15). Once again, the bonding between the iron and imide nitrogen is highly covalent thereby complicating the oxidation state assignment. Examination of the doubly occupied molecular orbitals reveals a low energy linear combination of the iron d_{xy} and imide nitrogen p_y orbitals that is 40% metal in character. Thus, an ambiguity arises where the metal may be assigned the +4 oxidation state as stated above or as an alternative, low-spin Fe(II) compound with a neutral nitrene ligand. The most accurate depiction of the compound is likely a resonance structure between these two extremes with a highly delocalized [FeNMe] fragment, akin to the bonding in metal nitrosyls.[45] Importantly, the XAS measurements on the

dx.doi.org/10.1021/ja205736m |*J. Am. Chem. Soc.* 2011, 133, 17353–17369

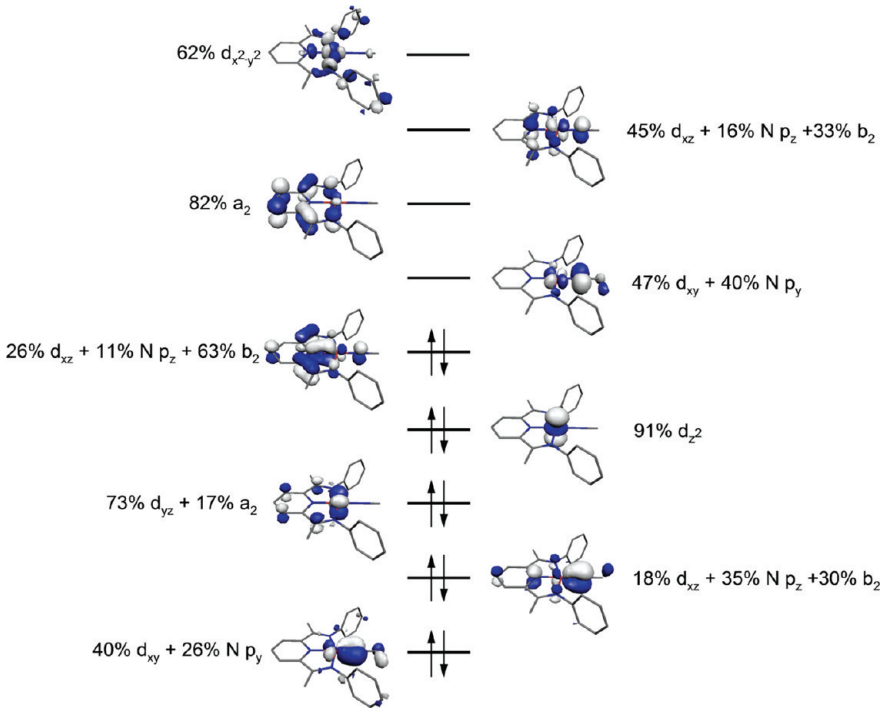

Figure 15. Molecular orbital diagram obtained from a restricted closed-shell calculation for (^{H}PDI)FeNMe (RKS $S = 0$).

experimental compound, (^{iPr}PDI)FeN^{1}Ad, are consistent with an average of these two extremes and give the appearance of an Fe(III) compound.

In addition to the closed-shell state, three singlet states arising from broken symmetry solutions were also evaluated (Figure 14). The BS(1,1) and BS(2,2) calculations converge to the same solution, corresponding to a BS(2,2) state, arising from two unpaired electrons on an intermediate spin ferrous center ($S_{Fe} = 1$) antiferromagnetically coupled to a $[PDI]^{1-}$ radical anion ($S_{PDI} = 1/2$) and an $[^{\bullet}NMe]^{1-}$ imidyl radical ($S_{imide} = 1/2$). The d_{yz} and d_{xy} orbitals on the iron are doubly occupied while the $d_{x^2-y^2}$ orbital is empty. The remaining d_{xz} and d_{z^2} orbitals are singly occupied. While the d_{xz} orbital has the appropriate symmetry to overlap with the singly occupied b_2 orbital of the bis(imino)-pyridine ligand resulting in antiferromagnetic coupling, the d_{z^2} orbital cannot interact with the unpaired electron of the imidyl radical, which is predominantly located in the p_y orbital of the imide nitrogen. Despite this unfavorable magnetic interaction, the BS(2,2) open-shell singlet solution is slightly lower in energy than the closed-shell singlet. It is computed to be only 9.5 kcal/mol higher in energy than the low-lying triplet solution. However, the computed singly reduced bis(imino)pyridine is inconsistent with the experimentally determined bond distances and is therefore discarded.

Finally, a BS(3,3) calculation yielded the lowest-energy singlet solution, lying only 7.6 kcal/mol above the low-energy triplet. Analysis of the resulting orbitals demonstrates that the iron center is best described as intermediate spin ferric (S_{Fe} =3/2) with a doubly occupied d_{z^2} orbital, three singly occupied orbitals (d_{xy}, d_{xz}, d_{yz}) and an empty $d_{x^2-y^2}$ orbital. Antiferromagnetic coupling of the electrons in the d_{xz} and d_{yz} orbitals with the b_2 and a_2 SOMO orbitals of the triplet ($S_{PDI} = 1$) bis(imino)pyridine diradical, respectively, and of the d_{xy} orbital with an imidyl radical ($S_{imide} = 1/2$) gives rise to the overall $S = 0$ state. However, high overlap values of 0.81 and 0.77 for the d_{yz} and d_{xy} orbitals with their corresponding orbitals on the ligands imply high covalency and lead to reduced spin density values.

Additional unrestricted DFT calculations revealed two other paramagnetic states. The lower in energy of the two is a quintet ($S = 2$) state that is nearly degenerate with the closed-shell, RKS ($S = 0$) solution, and is 13.3 kcal/mol above the lowest-energy triplet (Figure 14). Analysis of the orbital picture from this state revealed a similar electronic structure to the low-energy triplet with the principal difference arising from ferromagnetic rather than antiferromagnetic coupling between the unpaired spins on the iron and the bis(imino)pyridine radical. The second paramagnetic excited state is a septet (UKS, $S = 3$, Figure 14) and is well separated by 31.9 kcal/mol from the low-energy triplet. The Mulliken spin density indicates two unpaired spins on the bis(imino)pyridine ligand, e.g. $[PDI]^{2-}$, $S_{PDI} = 1$, three unpaired spins on the iron and one additional spin on the imide fragment.

In summary, the initial investigations based on the truncated model system with enforced C_{2v} symmetry reveal that a number of spin states may be accessible in a relatively narrow energy range. In contrast to the experimental data, the lowest-energy state is a triplet with a monoanionic bis(imino)pyridine. However, it has been shown that modern hybrid DFT functionals like B3LYP are slightly biased in favor of the high-spin state for SCO compounds and spin state alone should not be the only measure of the validity of the computational results.[44]

The computational results obtained from the model complex inspired the three approaches used for the full molecule: a restricted closed-shell singlet (RKS), an open-shell singlet BS-(3,3), and an open-shell triplet BS(3,1) calculation. Consistent with the calculations for (^{iPr}PDI)FeNDipp, geometry optimizations for (^{iPr}PDI)FeN^{1}Ad were initially carried out at the BP86 level of DFT without imposing geometric constraints. However, all attempts to obtain an open-shell singlet solution failed with

Table 5. Comparison of Selected Experimental and Computed Bond Distances (Å) and Angles (deg) for (^{iPr}PDI)FeN^{1}Ad

	experimental	BS(3,1)	BS(2,2)	RKS
Fe−N_{imide}	1.648(2)	1.727	1.774	1.629
Fe−N_{py}	1.895(2)	1.914	1.896	1.900
Fe−N_{imine}	1.933(1)	2.053	2.072	2.002
N_{imine}−C_{imine}	1.340(2)	1.325	1.324	1.331
C_{imine}−C_{ipso}	1.418(2)	1.443	1.442	1.428
N_{py}−Fe−N_{imide}	168.10(8)	171.21	169.35	166.23
Fe−N_{imide}−C_{ipso}	159.87(15)	160.29	155.82	168.50

this functional. Instead, the calculations converged back to a closed-shell singlet solution. This is a well-documented phenomenon for pure gradient functionals like BP86, which overestimate the stability of pure low-spin states.[46] Accordingly, the B3LYP functional was used for geometry optimizations for all three approaches. Note that in contrast to the calculations for (^{iPr}PDI)-FeNDipp, the obtained geometries for the BS(3,1) and the RKS approach were almost identical for both functionals in this case. Although the electronic structures obtained from the closed-shell singlet and the triplet computations were qualitatively identical to those obtained for the idealized planar model system, all attempts to generate a BS(3,3) solution failed. Instead, the molecule converged to a BS(2,2) solution that is different from the BS(2,2) solution described above. In contrast to the truncated model system, the two unpaired electrons on the iron(II) center are located in the d_{xz} and the d_{xy} orbitals, maximizing the overlap with the singly occupied b_2 orbital of the bis(imino)pyridine radical and the imidyl radical ligand.

Comparing the total energies of the three electronic structures, the triplet solution was the lowest in energy while the open-shell singlet (BS(2,2)) and the closed-shell singlet, were 7.1 and 18.1 kcal/mol higher in energy, respectively. This is again in agreement with the slight bias of modern hybrid DFT functionals toward high-spin states in SCO complexes.[44] A comparison of the computed structural parameters for each solution is reported in Table 5. In agreement with their electronic structures, the metrical parameters obtained from the triplet BS(3,1) and open-shell singlet BS(2,2) calculations exhibit bis(imino)pyridine bond distances indicative of a monoreduced $[PDI]^{1-}$ radical ligand. This is in conflict with the experimental bond distances, which indicate a doubly reduced $[PDI]^{2-}$ ligand. Furthermore, the Fe−N_{imide} and Fe−N_{imine} bond lengths are significantly overestimated by both solutions. In contrast, the closed-shell singlet solution (denoted RKS) exhibits much better agreement with the experimental structure (Table 5).

To further assay the validity of each solution, Mössbauer parameters were computed and compared to the experimentally determined values for (^{iPr}PDI)FeN^{1}Ad. These values are reported in Table 6. All three solutions successfully reproduce the experimental isomer shift, but the calculated quadrupole splittings vary widely. Most notably, the triplet BS(3,1) calculation yielded a relatively narrow and positive ΔE_Q, in disagreement with the experimental data. In fact, this value more closely resembles the values for the $S = 1$ aryl-substituted iron imides, (^{iPr}PDI)FeN*Ar*. By contrast, the two singlet solutions reproduce the negative quadrupole splitting. However, the magnitude of ΔE_Q is severely overestimated by the closed-shell (RKS) model,

Table 6. Comparison of Experimental and Computed Mössbauer Parameters for (^{iPr}PDI)FeN^{1}Ad

	experimental	BS(3,1)	BS(2,2)	RKS
δ/ mm·s^{-1}	0.04	0.09	0.04	0.01
ΔE_Q/ mm·s^{-1}	−2.38	1.29	−2.03	−4.08

while it is in good agreement for the broken-symmetry, BS(2,2) description.

Unfortunately, the computational results described above do not provide a conclusive description of the electronic ground state of (^{iPr}PDI)FeN^{1}Ad. Of all investigated models for the full molecule, the restricted closed-shell (RKS) solution best reproduces the experimental criteria listed at the beginning of the computational section. Most importantly, and in contrast to the two alternative descriptions, it reproduces the bond distances of the doubly reduced bis(imino)pyridine ligand. Furthermore, the diamagnetic low-spin configuration in both resonance structures (low-spin Fe(II), neutral nitrene ↔ low-spin Fe(IV), $[NR]^{2-}$) readily explains the very short Fe−N_{imine} and Fe−N_{imide} bonds and leads to a higher formal bond order for the Fe−N_{imide} bond as compared to the aryl-substituted iron imides. In contrast to the $S = 1$ and BS(2,2) solutions, the closed-shell RKS solution is in agreement with the experimentally observed diamagnetic ground state (at cryogenic temperatures) and the metal oxidation state observed by XAS (also recorded at cryogenic temperatures), respectively. Nevertheless, the relatively high energy of this solution and the deviation of the computed Mössbauer quadrupole splitting are problematic. Because none of the employed computational approaches consistently reproduces the structural and spectroscopic observables of the compound, it seems likely that the complexity of the electronic structure of (^{iPr}PDI)-FeN^{1}Ad is beyond the scope of the current, single-determinant DFT methodology applicable to systems of the given size.

Evaluation of Electronic Structure Possibilities. From the combination of spectroscopic data, metrical parameters from X-ray diffraction, magnetochemistry, and computational studies, a clear description of the electronic structure the aryl-substituted bis(imino)pyridine compounds has emerged. This class of molecules is best described as intermediate spin ferric compounds ($S_{Fe} = 3/2$) antiferromagnetically coupled to a bis(imino)pyridine radical anion with a traditional closed-shell imido fragment, $[NAr]^{2-}$. In this bonding description, four iron d-orbitals are populated giving rise to an Fe−N_{imide} bond order of 2 with two 2-center 3-electron π bonds, consistent with the long Fe−N bond distances of 1.705(2) (*Ar* = Dipp) and 1.717(2) Å (*Ar* = Mes) observed experimentally.

The electronic structure of the alkyl-substituted bis(imino)-pyridine iron imides is not as straightforward to interpret despite the same breadth of experimental and computational data. The combination of spin crossover behavior and two potentially redox active ligands, the bis(imino)pyridine and the imide fragment, complicate oxidation state assignment. Possibilities for the $S = 0$ ground states will be initially evaluated. Recall that the metrical parameters from X-ray diffraction establish two-electron chelate reduction in all cases, and therefore only electronic structures derived from these possibilities will be considered (Figure 16).

The most plausible electronic structure description for the $S = 0$ ground states of the bis(imino)pyridine iron *N*-alkyl-substituted imido complexes is a resonance structure between Fe(II) (**A**) and Fe(IV) (**B**). This depiction is supported computationally

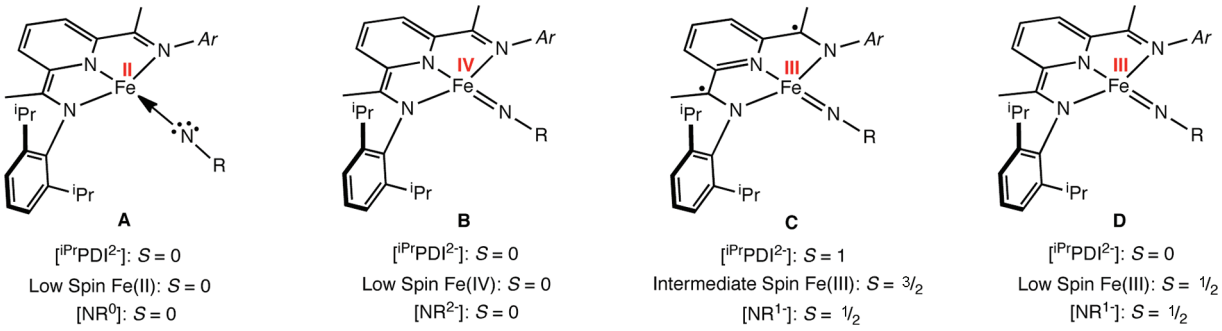

Figure 16. Electronic structure possibilities for *N*-alkyl-substituted bis(imino)pyridine imido compounds.

(Figure 15) and indicates a high degree of covalency between the iron and the bis(imino)pyridine and imide ligands. Such a bonding situation, often encountered with metal nitrosyls,[45] renders a single oxidation state assignment physically meaningless. With the present compounds, this is apparent from Mössbauer and X-ray data that are consistent with an Fe(IV) assignment (or low-spin Fe(II) and XAS measurements that detect the "hybrid" ferric form). These low-spin assignments, either Fe(II) or Fe(IV), account for the contracted $Fe-N_{imide}$ distances as well as the relatively short metal-chelate bond lengths. Two other Fe(III) possibilities, structures **C** and **D**, were also considered. Possibility **C**, with an intermediate spin ferric center ($S_{Fe} = 3/2$) antiferromagnetically coupled to both a imidyl radical and a triplet bis(imino)pyridine diradical, has been eliminated, as the Mössbauer isomer shift is too low for an intermediate spin Fe(III) compound. By contrast, possibility **D**, with a low-spin Fe(III) center antiferromangetically coupled to an imidyl radical is consistent with all of the experimental data and is a plausible electronic structure description for this class of compounds. We note that such an electronic structure description could not be reproduced computationally.

What is the electronic structure description for the $S = 1$ state of (^{iPr}PDI)Fe^{2}Ad? At first glance, one might conclude this compound has the same electronic structure as the $S = 1$ (^{iPr}PDI^{1-})Fe^{III}NAr class of molecules. While much of the high temperature ($T > 200$ K) experimental data for (^{iPr}PDI)Fe^{2}Ad begins to approach the values obtained for the (^{iPr}PDI^{1-})-Fe^{III}NAr derivatives, in many cases it remains sufficiently dissimilar, supporting yet another unique electronic structure. Recall that the metrical parameters from the X-ray data, collected at 253 K where the molecule is completely in its $S = 1$ form, establish a two-electron reduced bis(imino)pyridine chelate and a nearly planar molecule, features distinct from the *N*-aryl substituted imides. In addition, the Mössbauer parameters (δ = 0.19 mm·s^{-1} and $\Delta E_Q = |0.75|$ mm·s^{-1}) are lower than the aryl compounds (δ = 0.30 mm·s^{-1} and $\Delta E_Q = +1.08$ and $|1.34|$ mm·s^{-1}). Unfortunately, due to the limitations of applied field Mössbauer spectroscopy the sign of the quadrupole splitting for the $S = 1$ state of (^{iPr}PDI)Fe^{2}Ad cannot be experimentally determined. One possibility for the $S = 1$ state of (^{iPr}PDI)Fe^{2}Ad is an intermediate spin Fe(IV) (or intermediate spin Fe(II)) compound with closed-shell dianionic, $[PDI]^{2-}$ and $[N^{2}Ad]^{2-}$, ligands. An alternative and equally plausible possibility is an intermediate spin ferric compound ($S_{Fe} = 3/2$) antiferromagnetically coupled to an imidyl radical ($S_{imide} = 1/2$) with a closed-shell dianionic chelate. The observation of a higher Mössbauer isomer shift for the $S = 1$ spin isomer supports these possibilities. Given all of the experimental and computational data, this electronic structure, along with structure **D** in Figure 16, are the preferred electronic structures for (^{iPr}PDI)Fe^{2}Ad.

One final question is why do the electronic structures of the bis(imino)pyridine iron imides vary as a function of the *N*-imido substituent? The current data are most consistent with a steric effect that in turn triggers electronic structure differences. Both the $Fe-N_{imide}$ distance and vector (in-plane versus out-of-plane) are determined by the size of the imido substituent, where the larger 2,6-disubstituted aryl groups lift out of the iron−chelate plane to avoid steric interactions with the bis(imino)pyridine aryl substituents. Accordingly, the iron−nitrogen overlap decreases, resulting in an overall weaker field interaction giving rise to a one-electron reduced bis(imino)pyridine and higher spin state at iron. For the *N*-alkyl substituted cases, the Fe−NR fragment can lie between the chelate aryl substituents and increase orbital overlap with the metal, increasing its covalency and, accordingly, its field strength, resulting in a two-electron reduced chelate and a low-spin iron center. These effects highlight the true redox flexibility of the bis(imino)pyridine chelate and the ability to accept electron density in response to the field strength of a *trans* (or pseudo-*trans*) ligand.

EXPERIMENTAL SECTION

General Considerations. All air- and moisture-sensitive manipulations were carried out using standard vacuum line, Schlenk, and cannula techniques or in an MBraun inert atmosphere drybox containing an atmosphere of purified nitrogen. Solvents for air- and moisture-sensitive manipulations were initially dried and deoxygenated using literature procedures. Benzene-d_6 was purchased from Cambridge Isotope Laboratories and dried over 4 Å molecular sieves. The iron complexes, (^{iPr}PDI)Fe$(N_2)_2$,[22] (^{iPr}PDI)FeNDipp,[26] and (^{iPr}PDI)FeNMes,[26] were prepared as described previously.

^{1}H NMR spectra were recorded on Varian Mercury 300, Inova 400, and 500 spectrometers operating at 299.76, 399.78, and 500.62 MHz, respectively. All ^{1}H chemical shifts are reported relative to $SiMe_4$ using the ^{1}H (residual) shift of the solvent as a secondary standard. Variable temperature (2−300 K) magnetization data were recorded in a 1 T magnetic field on a MPMS Quantum Design SQUID magnetometer. The experimental magnetic susceptibility data were corrected underlying diamagnetism using tabulated Pascal's constants.[48] Elemental analyses were performed at Robertson Microlit Laboratories, Inc., in Madison, NJ.

X-ray crystallographic data were collected at 173 K on a Bruker X8 APEX2 diffractometer diffractometer using graphite monochromated Mo Kα radiation (λ = 0.71073 Å), 100 K on a Bruker D8 Avance

diffractometer using graphite monochromated Mo Kα or Cu Kα radiation (λ = 1.54178 Å). A hemisphere routine was used for data collection and determination of lattice constants. The space group was identified and the data were processed using the Bruker SAINT+ program and corrected for absorption using SADABS. The structures were solved using direct methods completed by subsequent Fourier synthesis and refined by full-matrix least-squares procedures. Unless otherwise stated, all non-hydrogen atoms were refined with anisotropic displacement parameters and hydrogen atoms were placed using a riding model and refined with fixed isotropic displacement parameters. The crystal structure of (^{iPr}PDI)FeN^{Cy}Oct was of poor data quality and was collected at the Cornell High Energy Synchroton Source (CHESS) at λ = 0.97820 Å at 293 K.

Zero-field ^{57}Fe Mössbauer data were recorded on a SEE Co. Mössbauer spectrometer (MS4) at 80 K in constant acceleration mode, using ^{57}Co/Rh as the radiation source. The minimum experimental line width was 0.24 mm s^{-1} (full width at half-height). Zero-field Mössbauer spectra were simulated with the program WMOSS (least-squares fitting to Lorentzian peaks). The temperature of the samples was controlled by a Janis Research Co. CCS-850 He/N_2 cryostat within an accuracy of ±0.3 K. Applied field Mössbauer data were collected using an Oxford Instruments Mössbauer-Spectromag cryostat, where the split-pair superconducting magnet system allows applied fields up to 8 T and the temperature of the samples can be varied in the range of 1.5−250 K. The field at the sample is perpendicular to the γ beam. Magnetic Mössbauer spectra were simulated with the program MX (by Eckhard Bill). Isomer shifts for all spectra were determined relative to α-iron at 298 K.

XAS data were recorded at the Stanford Synchrotron Radiation Laboratory (SSRL) on focused beamline 9-3, under ring conditions of 3 GeV and 60−100 mA. A Si(220) double-crystal monochromator was used for energy selection, and a Rh-coated mirror (set to an energy cutoff of 10 keV) was used for harmonic rejection. Internal energy calibration was performed by assigning the first inflection point of the Fe foil spectrum to 7111.2 eV. Samples were prepared by dilution in boron nitride, pressed into a pellet and sealed between 38 μm Kapton tape windows in a 1-mm aluminum spacer. All samples were maintained at 10 K during data collection using an Oxford Instruments CF1208 continuous flow liquid helium cryostat. Data were measured in transmission using nitrogen-filled ionization chambers. The data were calibrated and averaged using EXAFSPAK.[49] Normalization of the data was achieved by subtracting the spline and normalizing the postedge region to 1.

Computational Details. All DFT calculations were performed with the ORCA program package[50] using the BP86[51−53] or B3LYP[51,54,55] functionals.[56] The all-electron Gaussian basis sets were those developed by the Ahlrichs group.[57−59] Triple-ζ quality basis sets def2-TZVP with one set of polarization functions on iron and on the atoms directly coordinated to the metal center were used. For the carbon and hydrogen atoms, slightly smaller polarized split-valence def2-SV(P) basis sets were used, that were of double-ζ quality in the valence region and contained a polarizing set of d-functions on the non-hydrogen atoms. Auxiliary basis sets were chosen to match the orbital basis.[60−62] The RIJCOSX[63−65] approximation was used to accelerate the calculations.

Throughout this paper we describe our computational results by using the broken-symmetry (BS) approach by Ginsberg[66] and Noodleman.[67] Because several broken symmetry solutions to the spin-unrestricted Kohn−Sham equations may be obtained, the general notation BS(m,n)[68] has been adopted, where m (n) denotes the number of spin-up (spin-down) electrons at the two interacting fragments. Canonical and corresponding[69] orbitals, as well as spin density plots, were generated with the program Molekel.[70]

Nonrelativistic single-point calculations on the optimized geometry were carried out to predict Mössbauer spectral parameters (isomer shifts and quadrupole splittings). These calculations employed the CP(PPP) basis set for iron.[71] The Mössbauer isomer shifts were calculated from the computed electron densities at the iron centers as previously described.[72,73]

Preparation of (^{iPr}PDI)FeN^{1}Ad. A 20-mL scintillation vial was charged with 0.094 g (0.174 mmol) of (^{iPr}PDI)Fe(N_2)$_2$ and approximately 15 mL of pentane forming a dark green solution. A solution of 0.028 g (0.174 mmol) 1-adamantyl azide in 3 mL of pentane was prepared and added dropwise to the vial, resulting in a gradual color change of the solution from green to purple. The resulting solution was stirred for 15 min then filtered through a glass frit. The purple solution was cooled to −35 °C to yield 0.065 g (60%) of purple diamond-shaped crystals identified as (^{iPr}PDI)FeN^{1}Ad. Analysis for $C_{43}H_{58}N_4Fe$: Calc. C, 75.20; H, 8.51; N, 8.16. Found C, 74.82; H, 8.49; N, 7.80. ^{1}H NMR (benzene-d_6, 20 °C): δ = −15.25 (s, 6H, C(CH_3)), −6.72 (br s, 4H, CH(CH_3)$_2$), −1.23 (br s, 12H, CH(CH_3)$_2$), −0.48 (br s, 12H, CH(CH_3)$_2$), 2.54 (br s, 6H, adamantyl CH_2), 3.05 (d, 12 Hz, 3H, adamantyl CH_2), 3.88 (d, 12 Hz, 3H, adamantyl CH_2), 6.03 (d, 8 Hz, 4H, *m-aryl*), 7.27 (t, 8 Hz, 2H, *p-aryl*), 9.27 (br s, 3H, adamantyl CH_2), 16.41 (br s, 2H, *m-pyridine*), 22.30 (br s, 1H, *p-pyridine*). ^{1}H NMR (toluene-d_8, −80 °C): −0.06 (s, 6H, C(CH_3)), 0.56 (br s, 12H, CH(CH_3)$_2$), 0.61 (br s, 12H, CH(CH_3)$_2$), 1.44 (br s, 6H, adamantyl CH_2), 1.65 (br s, 4H, CH(CH_3)$_2$), 1.82 (br s, 3H, adamantyl CH_2), 2.45 (br s, 3H, adamantyl CH_2), 2.75 (br s, 3H, adamantyl CH_2), 6.76 (br s, 4H, *m-aryl*), 7.10 (br s, 2H, *p-aryl*), 8.75 (br s, 2H, *m-pyridine*), 9.27 (br s, 1H, *p-pyridine*). ^{13}C {^{1}H} NMR (benzene-d_6): δ = 20.61, 20.78, 29.93, 30.11, 33.39, 42.66, 42.93, 71.40, 95.52, 100.41, 117.73, 124.05, 124.23, 140.92, 178.98, 202.17.

Preparation of (^{iPr}PDI)FeN^{Cy}Oct. This compound was prepared in the same manner as (^{iPr}PDI)FeN^{1}Ad with 0.244 g (0.411 mmol) of (^{iPr}PDI)Fe(N_2)$_2$ and 0.057 g (0.372 mmol) of cyclooctyl azide and yielded 0.243 g (86%) of dark-purple crystals identified as (^{iPr}PDI)-FeN^{Cy}Oct. Analysis for $C_{41}H_{58}N_4Fe$: Calc. C, 74.30; H, 8.82; N, 8.45. Found C, 74.67; H, 8.80; N, 7.97. ^{1}H NMR (benzene-d_6): δ = −16.36 (s, 6H, C(CH_3)), −6.31 (br s, 4H, CH(CH_3)$_2$), −0.96 (br s, 12H, CH(CH_3)$_2$), −0.24 (br s, 12H, CH(CH_3)$_2$), 3.26 (m, 1H, cyclooctyl CH), 3.90 (m, 8H, cyclooctyl CH_2), 4.07 (m, 2H, cyclooctyl CH_2), 4.58 (m, 2H, cyclooctyl CH_2), 5.48 (m, 2H, cyclooctyl CH_2), 6.17 (d, 7.5 Hz, 4H, *m-aryl*), 7.40 (t, 7.5 Hz, 2H, *p-aryl*), 18.02 (br s, 2H, *m-pyridine*), 20.64 (br s, 1H, *p-pyridine*). {^{1}H}^{13}C NMR (benzene-d_6): δ = 20.31, 31.84, 33.94, 34.37, 39.96, 72.71, 76.49, 106.04, 118.36, 124.22, 126.73, 136.45, 166.14, 189.59, 210.32.

Preparation of (^{iPr}PDI)FeN^{2}Ad. This compound was prepared in the same manner as (^{iPr}PDI)FeN^{1}Ad with 0.103 g (0.174 mmol) of (^{iPr}PDI)Fe(N_2)$_2$, approximately 15 mL of pentane, and 0.031 g (0.174 mmol) of 2-adamantyl azide and yielded 0.087 g (73%) of black crystals identified as (^{iPr}PDI)FeN^{2}Ad. Analysis for $C_{43}H_{58}N_4Fe$: Calc. C, 75.20; H, 8.51; N, 8.16. Found C, 74.78; H, 7.75; N, 7.83. Magnetic susceptibility (benzene-d_6, 293 K): μ_{eff} = 2.8(1) μ_B. ^{1}H NMR (benzene-d_6): δ = −121.05 (152.0 Hz, 6H, C(CH_3)), −56.34 (273.0 Hz, 4H, CH(CH_3)$_2$), −12.11 (91.7 Hz, 12H, CH(CH_3)$_2$), −7.30 (44.6 Hz, 12H, CH-(CH_3)$_2$), −0.03 (47.8 Hz, 4H), 7.87 (40.0 Hz, 2H), 12.07 (36.3 Hz, 2H), 14.07 (77.5 Hz, 4H), 21.68 (101.0 Hz, 4H), 21.95 (156.2 Hz, 2H), 60.74 (204.7 Hz, 2H), 72.80 (110.4 Hz, 2H, *m-pyridine*), 94.01 (104.3 Hz, 1H, adamantyl or *p-pyridine*), one resonance not located.

■ ASSOCIATED CONTENT

Supporting Information. Additional variable-temperature NMR data, Eyring plot, computational results, and crystallographic data for (^{iPr}PDI)FeN^{1}Ad, (^{iPr}PDI)FeN^{Cy}Oct, and (^{iPr}PDI)-FeN^{2}Ad in CIF format. This material is available free of charge via the Internet at http://pubs.acs.org.

■ AUTHOR INFORMATION

Corresponding Author
pchirik@princeton.edu

■ ACKNOWLEDGMENT

We thank U.S. National Science Foundation and Deutsche Forschungsgemeinschaft for a Cooperative Activities in Chemistry between U.S. and German Investigators grant. S.D. thanks the Department of Chemistry and Chemical Biology at Cornell University for financial support. SSRL operations are funded by the Department of Energy, Office of Basic Energy Sciences. The Structural Molecular Biology program is supported by the National Institutes of Health, National Center for Research Resources, Biomedical Technology Program and by the Department of Energy, Office of Biological and Environmental Research. We also thank Jon Darmon for preparation of the Table of Contents graphic.

■ REFERENCES

(1) Mehn, M. P.; Peters, J. C. *Inorg. Biochem.* **2006**, *100*, 634.
(2) Berry, J. F. *Prog. Inorg. Chem.* **2009**, *30*, 28.
(3) Verma, A. K.; Nazif, T. N.; Achim, C.; Lee, S. C. *J. Am. Chem. Soc.* **2000**, *122*, 11013.
(4) Ni, C.; Fettinger, J. C.; Long, G. J.; Brynda, M.; Power, P. P. *Chem. Commun.* **2008**, 6045.
(5) Brown, S. D.; Peters, J. C. *J. Am. Chem. Soc.* **2005**, *127*, 1913.
(6) Brown, S. D.; Betley, T. A.; Peters, J. C. *J. Am. Chem. Soc.* **2003**, *125*, 322.
(7) Thomas, C. M.; Mankad, N. P.; Peters, J. C. *J. Am. Chem. Soc.* **2006**, *128*, 4956.
(8) Mankand, N. P.; Müller, P.; Peters, J. C. *J. Am. Chem. Soc.* **2010**, *132*, 4083.
(9) Moret, M.-E.; Peters, J. C. *Angew. Chem., Int. Ed.* **2011**, *50*, 2063.
(10) Brown, S. D.; Peters, J. C. *J. Am. Chem. Soc.* **2004**, *126*, 4538.
(11) Nieto, I.; Ding, F.; Bontchev, R. P.; Wang, H.; Smith, J. M. *J. Am. Chem. Soc.* **2008**, *130*, 2716.
(12) Eckert, N. A.; Vaddadi, S.; Stoian, S.; Lachicotte, R. J.; Cundari, T. R.; Holland, P. L. *Angew. Chem., Int. Ed.* **2006**, *45*, 6868.
(13) Cowley, R. E.; DeYonker, N. J.; Eckert, N. A.; Cundari, T. R.; DeBeer, S.; Bill, E.; Ottenwaelder, X.; Flaschenriem, C.; Holland, P. L. *Inorg. Chem.* **2010**, *49*, 6172.
(14) Cowley, R. E.; Holland, P. L. *Inorg. Chim. Acta* **2011**, *369*, 40.
(15) Cowley, R. E.; Eckert, N. A.; Vaddadi, S.; Figg, T. M.; Cundari, T. R.; Holland, P. L. *J. Am. Chem. Soc.* **2011**, *133*, 9796.
(16) Cowley, R. E.; Elhaïk, J.; Eckert, N. A.; Brennessel, W. W.; Bill, E.; Holland, P. L. *J. Am. Chem. Soc.* **2008**, *130*, 6074.
(17) Cowley, R. E.; Eckert, N. A.; Elhaïk, J.; Holland, P. L. *Chem. Commun.* **2009**, 1760.
(18) King, E. R.; Betley, T. A. *Inorg. Chem.* **2009**, *48*, 2361.
(19) King, E. R.; Hennessey, E. T.; Betley, T. A. *J. Am. Chem. Soc.* **2011**, *133*, 4917.
(20) Lu, C. C.; George, S. D.; Weyhermüller, T.; Bill, E.; Bothe, E.; Wieghardt, K. *Angew. Chem., Int. Ed.* **2008**, *47*, 6384.
(21) Lucas, R. L.; Powell, D. R.; Borovik, A. S. *J. Am. Chem. Soc.* **2005**, *127*, 11596.
(22) Bart, S. C.; Lobkovsky, E.; Chirik, P. J. *J. Am. Chem. Soc.* **2004**, *126*, 13794.
(23) Chirik, P. J.; Wieghardt, K. *Science* **2010**, *327*, 794.
(24) Bart, S. C.; Chlopek, K.; Bill, E.; Bouwkamp, M. W.; Lobkovsky, E.; Neese, F.; Wieghardt, K.; Chirik, P. J. *J. Am. Chem. Soc.* **2006**, *128*, 13901.
(25) Knijnenburg, Q.; Gambarotta, S.; Budzelaar, P. H. M. *Dalton Trans.* **2006**, 5442.
(26) Bart, S. C.; Lobkovsky, E.; Bill, E.; Chirik, P. J. *J. Am. Chem. Soc.* **2006**, *128*, 5302–5303.
(27) (a) Fryzuk, M. D.; Love, J. B.; Rettig, S. J.; Young, V. G. *Science* **1997**, *275*, 1445. (b) Pool, J. A.; Lobkovsky, E.; Chirik, P. J. *Nature* **2004**, *427*, 527. (c) Pool, J. A.; Bernskoetter, W. H.; Chirik, P. J. *J. Am. Chem. Soc.* **2004**, *126*, 14326. (d) Bernskoetter, W. H.; Lobkovsky, E.; Chirik, P. J. *J. Am. Chem. Soc.* **2005**, *127*, 14051.
(28) Bowman, A. C.; Bart, S. C.; Heinemann, F. W.; Meyer, K.; Chirik, P. J. *Inorg. Chem.* **2009**, *48*, 5587.
(29) Cowley, R. E.; Bill, E.; Neese, F.; Brennessel, W. W.; Holland, P. L. *Inorg. Chem.* **2009**, *48*, 4828.
(30) Bowman, A. C. Ph. D. Thesis, Cornell University 2010.
(31) Knijnenburg, Q.; Hetterscheid, D.; Kooistra, T. M.; Budzelaar, P. H. M. *Eur. J. Inorg. Chem.* **2004**, 1204.
(32) Kahn, O. *Molecular Magnetism*; VCH: New York, 1993.
(33) Sorai, M.; Seki, S. *J. Phys. Chem. Solids* **1974**, *35*, 555.
(34) Long, G. J. Mössbauer spectroscopy as a structural probe. In *Mössbauer Spectroscopy*; Dickson, D. P. E., Berry, F. J., Eds.; Cambridge University Press: Cambridge, 1986; p 70.
(35) Gütlich, P. Spin crossover in iron(II)-complexes. In *Metal Complexes*; Clarke, M. J., Hemmerich, P., Jørgensen, C. K., Reinen, D., Williams, R. J. P., Eds.; Springer-Verlag: Berlin, 1981; Vol. 44, p 83.
(36) Gütlich, P.; Goodwin, H. A. Spin Crossover – An Overall Perspective. In *Spin Crossover in Transition Metal Compounds I*; Gütlich, P., Goodwin, H. A., Eds.; Springer-Verlag: Berlin, 2004; Vol. 233; p 1.
(37) Ginsberg, A. P. *J. Am. Chem. Soc.* **1980**, *102*, 111.
(38) Noodleman, L.; Peng, C. Y.; Case, D. A.; Mouesca, J. M. *Coord. Chem. Rev.* **1995**, *144*, 199.
(39) Kirchner, B.; Wennmohs, F.; Ye, S.; Neese, F. *Curr. Opin. Chem. Biol.* **2007**, *11*, 134.
(40) Berry, J. F.; DeBeer George, S.; Neese, F. *Phys. Chem. Chem. Phys.* **2008**, *10*, 4361.
(41) de Visser, S. P. *J. Am. Chem. Soc.* **2007**, *129*, 6168.
(42) Sinnecker, S.; Slep, L. D.; Bill, E.; Neese, F. *Inorg. Chem.* **2005**, *44*, 2245.
(43) Römelt, M.; Ye, S.; Neese, F. *Inorg. Chem.* **2009**, *48*, 784.
(44) Ye, S. F.; Neese, F. *Inorg. Chem.* **2010**, *49*, 772.
(45) Ye, S. F.; Neese, F. *J. Am. Chem. Soc.* **2010**, *132*, 3646.
(46) (a) Rong, C.; Lian, S.; Yin, D.; Shen, B.; Zhong, A.; Liu, S. *J. Chem. Phys.* **2006**, *125*, 174102. (b) Rong, C.; Lian, S.; Yin, D.; Zhong, A.; Zhang, R.; Liu, S. *Chem. Phys. Lett.* **2007**, *434*, 149.
(47) Alvarez, S. G.; Alvarez, M. T. *Synthesis* **1997**, 413–414.
(48) Bain, G. A.; Berry, J. F. *J. Chem. Ed.* **2008**, *85*, 532.
(49) George, G. N. *EXAFSPAK*, Stanford Synchrotron Radiation Laboratory, Stanford Linear Accelerator Center, Stanford University: Stanford, CA.
(50) Neese, F., Orca - an ab initio, DFT and Semiempirical Electronic Structure Package, Version 2.8, Revision 2287; *Institut für Physikalische und Theoretische Chemie*, Universität Bonn, Bonn (Germany), November 2010.
(51) Becke, A. D. *J. Chem. Phys.* **1986**, *84*, 4524.
(52) Perdew, J. P.; Yue, W. *Phys. Rev. B* **1986**, *33*, 8800.
(53) Perdew, J. P. *Phys. Rev. B* **1986**, *33*, 8822.
(54) Becke, A. D. *J. Chem. Phys.* **1993**, *98*, 5648.
(55) Lee, C. T.; Yang, W. T.; Parr, R. G. *Phys. Rev. B* **1988**, *37*, 785.
(56) The BP86 functional is a pure DFT functional, which includes the generalized gradient approximation (GGA). Generally, this functional has been shown to give good results for optimized geometries at relatively low computational cost. Pure GGA-functionals, however, suffer from difficulties in expressing the exchange part of the total energy, which is particularly problematic for exchange-coupled systems as presented in this work. Therefore, all electronic structure descriptions and calculations of spectroscopic parameters presented in this work were obtained from computations using the B3LYP functional. This hybrid DFT functional includes a component of exact exchange energy calculated by Hartree−Fock theory. For all geometry optimizations with BP86 we carefully checked that the electronic structure obtained by this functional was qualitatively identical to the B3LYP solution.
(57) Schäfer, A.; Horn, H.; Ahlrichs, R. *J. Chem. Phys.* **1992**, *97*, 2571.
(58) Schäfer, A.; Huber, C.; Ahlrichs, R. *J. Chem. Phys.* **1994**, *100*, 5829.
(59) Weigend, F.; Ahlrichs, R. *Phys. Chem. Chem. Phys.* **2005**, *7*, 3297.
(60) Eichkorn, K.; Weigend, F.; Treutler, O.; Ahlrichs, R. *Theory Chem. Acc.* **1997**, *97*, 119.

(61) Eichkorn, K.; Treutler, O.; Öhm, H.; Häser, M.; Ahlrichs, R. *Chem. Phys. Lett.* **1995**, *240*, 283.
(62) Eichkorn, K.; Treutler, O.; Öhm, H.; Häser, M.; Ahlrichs, R. *Chem. Phys. Lett.* **1995**, *242*, 652.
(63) Neese, F.; Wennmohs, F.; Hansen, A.; Becker, U. *Chem. Phys.* **2009**, *356*, 98.
(64) Kossmann, S.; Neese, F. *Chem. Phys. Lett.* **2009**, *481*, 240.
(65) Neese, F. *J. Comput. Chem.* **2003**, *24*, 1740.
(66) Ginsberg, A. P. *J. Am. Chem. Soc.* **1980**, *102*, 111.
(67) Noodleman, L.; Peng, C. Y.; Case, D. A.; Mouesca, J. M. *Coord. Chem. Rev.* **1995**, *144*, 199.
(68) Kirchner, B.; Wennmohs, F.; Ye, S.; Neese, F. *Curr. Opin. Chem. Biol.* **2007**, *11*, 134.
(69) Neese, F. *J. Phys. Chem. Solids* **2004**, *65*, 781.
(70) Molekel, Advanced Interactive 3D-Graphics for Molecular Sciences, available under http://www.cscs.ch/molkel/.
(71) Neese, F. *Inorg. Chim. Acta* **2002**, *337*, 181.
(72) Sinnecker, S.; Slep, L. D.; Bill, E.; Neese, F. *Inorg. Chem.* **2005**, *44*, 2245.
(73) Römelt, M.; Ye, S.; Neese, F. *Inorg. Chem.* **2009**, *48*, 784.